Ocean Heat Uptake in Eddying and Non-eddying Ocean Circulation Models in a Warming Climate

YU ZHANG * AND GEOFFREY K. VALLIS

Princeton University, Princeton NJ 08540

J. Phys. Oceanography (in press)

*Corresponding author address: Yu Zhang, 201 Forrestal Rd., Princeton, NJ 08540

E-mail: yuz@princeton.edu

ABSTRACT

Ocean heat uptake is explored with non-eddying (2°), eddy-permitting (0.25°) and eddy-resolving (0.125°) ocean circulation models in a domain crudely representing the Atlantic basin connected to a southern circumpolar channel with flat bottom. The model is forced with a wind stress and a restoring condition for surface buoyancy that is linearly dependent on temperature, both being constant (in time) in the control climate. When the restore temperature is instantly enhanced regionally, two distinct processes are found relevant for the ensuing heat uptake: heat uptake into the ventilated thermocline forced by Ekman pumping and heat absorption in the deep ocean through meridional overturning circulation (MOC). Temperature increases in the thermocline occur on the decadal timescale whereas, over most of the abyss, it is the millennial time scale that is relevant, and the strength of MOC in the channel matters for the intensity of heat uptake. Under global, uniform warming, the rate of increase of total heat content increases with both diapycnal diffusivity and strengthening southern ocean westerlies.

In models with different resolutions, ocean responses to uniform warming share similar patterns with important differences. The transfer by mesoscale eddies is insufficiently resolved in the eddy-permitting model, resulting in steep isopycnals in the channel and weak lower MOC, and this in turn leads to weaker heat uptake in the abyssal ocean. Also, the reduction of the northern-hemisphere meridional heat flux (that occurs in a warmer world because of a weakening of MOC) increases with resolution. Consequently, the cooling tendency near the polar edge of the subtropical gyre is most significant in the eddy-resolving model.

1. Introduction

Because of its large specific heat capacity the ocean is an immense reservoir of heat[1] and more than 80% of the total increase of heat content in the Earth system between $1955-1998$ resides in the ocean (Levitus et al. 2005). The associated heat uptake is crucial in regulating and delaying global climate changes and has strong impacts on the sea-level rise that occurs from thermal expansion.

Greenhouse gases, such as carbon dioxide and methane, are well mixed in the atmosphere, but the distribution of the oceanic warming has been found to be rather non-uniform (Levitus et al. 2005, 2000). It has been suggested that changes in ocean circulation are significant in producing the spatial pattern of ocean heat uptake (Banks and Gregory 2006; Xie and Vallis 2011). Indeed, the oceanic meridional overturning circulation (MOC) has been found to slow down in a warming climate in a number of models (Gregory et al. 2005; Stouffer et al. 2006a) and (albeit with much more uncertainty) in observations (Bryden et al. 2005), and this reduction seems very likely to affect heat uptake by the ocean (Gregory 2000; Röuhlemann et al. 2004). More recently, by comparing the response to increasing CO_2 in two pairs of climate models, Rugenstein et al. (2013) suggested that models with a stronger MOC in control climate may have a stronger heat uptake in warming scenarios and possibly a greater reduction of the MOC.

Despite all these efforts, our understanding of the subject is far from complete. Indeed, even the basic mechanism driving heat uptake remains obscure. For example, it is not clear which factor, the rate of the MOC in the control climate, its reduction in a warmer world, or both, principally determines the rate of heat uptake. Although the factors that determine the strength of the MOC (such as the diapycnal diffusivity, mesoscale eddy activity and the winds over the Southern Ocean) are now becoming much better understood (e.g., Gnanadesikan 1999; Nikurashin and Vallis 2011, 2012), whether and how these same factors affect the distribution of heat uptake remain open questions. Mesoscale eddies are certainly important in regions like the Antarctic Circumpolar Current (ACC) (Speer et al. 2000; Henning and Vallis 2005; Radko and Marshall 2006) and the high-latitude convection sites (Spall 2004; Visbeck et al. 1997; Marshall and Schott 1999), but seem

[1] We use the word 'heat' as a convenient shorthand for internal energy.

to be likely less important in the center of gyres.

Interplay among the eddy transfer in the ACC and other elements such as the Southern Ocean westerlies, may play, through maintaining the MOC and producing deep ocean stratification (Gnanadesikan 1999; Wolfe and Cessi 2010, 2011; Nikurashin and Vallis 2012), a key role in ocean heat uptake. However, typical models in current climate research have fairly coarse resolutions with a grid size comparable to or bigger than the deformation radius, and must rely on a parameterization for representing eddy effects. The ocean heat uptake resolved from these models is therefore model dependent the vertical distribution of ocean heat uptake may be quite sensitive to the parameterized along-isopycnal eddy mixing (Huang et al. 2003). As computer resources increase ocean climate models are becoming 'eddy permitting', potentially partly resolving baroclinic eddies. The effects of resolution on heat uptake in the model ocean then becomes a question of great importance. In addition to ocean circulation, other mechanisms are also likely to be important for ocean heat uptake. For example, it was found in a model study that freshening from changes in ice will make surface water more stable, leading to weakening of the convection that is important in the deep ocean warming in the Southern Ocean (Bitz et al. 2006).

Among all these aforementioned issues, in this paper we are concerned with the response of the ocean circulation in a warming climate and its relation to ocean heat uptake. Certainly other effects may be important, but in order to focus on oceanic processes we use an ocean-only circulation model with an idealized configuration. We will show, with idealized experiments with surface warming in different regions, that there are two main oceanic mechanisms driving the heat uptake: one is tied to MOC and the other is related to Ekman pumping into the ventilated thermocline. Which mechanism is dominant depends on the geographical distribution of the surface warming. Heat uptake driven by these two mechanisms differ notably in many aspects such as strength, spatial pattern, and time scale. We investigate the ocean responses to surface warming in coarse-resolution (2°), eddy-permitting (0.25°) and eddy-resolving models (0.125°). In the course-resolution model we use a standard parameterization for mesoscale eddies, but have no parameterization in the other two models. Model resolution is found to be important. Thus, for example, in the eddy-permitting

model the isopycnals in the Southern Ocean are too steep and the lower MOC cell is correspondingly too weak, leading to a smaller heat uptake into the abyssal ocean compared to the eddy resolving model. We also find that the near surface cooling tendency around the polar edge of the subtropical gyre is strongest in the highest resolution model.

The paper is organized as follows. We first briefly describe the observations and current theory for the MOC in Section 2. An outline of the model and the experiments is given in Section 3. The mechanisms of ocean heat uptake are discussed using experiments with regional warming in the coarse-resolution model in Section 4. The ocean responses to uniform (i.e., uniform increase of restore temperature everywhere) warming in models with different resolutions are discussed and compared in Section 5. The sensitivity of heat uptake to diapycnal diffusivity and Southern Ocean westerlies is investigated in Section 6, followed by a conclusion in Section 7.

2. Meridional Overturning Circulation

The meridional overturning circulation (MOC) consists of a small number of cells each associated with water masses at different depths. Dominant are two inter-hemispheric, counter-rotating meridional cells below the main pycnocline (Fig. 1). One of the cells is at mid-depth, associated with isopycnals outcropping in both Northern Hemisphere and the ACC, and the other is an abyssal cell related to isopycnals ventilating only in the ACC or southwards of it. We henceforth call these the upper and lower MOC cell respectively. In the Atlantic Ocean, the northern branch of upper cell consists of sinking water forming North Atlantic Deep Water (NADW), followed by some upwelling at lower latitudes enabled by diapycnal mixing as well as a more adiabatic upwelling along sloping isopycnals in the ACC. The lower cell is composed of the sinking of Antarctic Bottom Water (AABW) around Antarctic and diapycnal mixing that is usually weak but is intensified above rough topography. Isopycnals outside the convection and outcropping regions are nearly flat, maintained by diffusion of heat from above and advection via diapycnal mixing from below. Between the two cells exists a thermostad, a weakly stratified water mass. Apart from the two global cells, there are

two smaller cells above the main pycnocline, in association with wind-driven subtropical gyres.

Within the transformed Eulerian mean framework (Andrews and McIntyre 1976), the overturning circulation, especially in the ACC region, is the 'residual' of a mean Eulerian circulation $\bar{\psi}$ and an eddy-driven overturning circulation ψ^*. Away from the region of the ACC, the eddy effects are thought to be generally small and the MOC is effectively just the Eulerian circulation, whereas in the ACC the two components do cancel to some degree. The Eulerian circulation, induced by the surface westerly winds, is proportional to $-\tau_s/f$ where τ_s is the westerly wind stress and f is the Coriolis parameter. The eddy-induced circulation is induced by eddies spawned from baroclinic instability of sloping isopycnals; it acts to slump the isopycnals and counteracts the overturning tendency of $\bar{\psi}$. In coarse-resolution models, ψ^* is typically parameterized as $K_e s$ where K_e is the eddy diffusivity of isopycnal thickness and $s = -\partial_y \bar{b}/\partial_z \bar{b}$ denotes the slope of buoyancy surface. A theory of the structure and amplitude of the two cells was recently presented by Nikurashin and Vallis (2012), and one aspect of that theory will be particularly relevant for us. The upper cell is driven by a combination of Southern Ocean winds and diapycnal mixing, whereas the lower cell is primarily mixing driven. The strength of the mixing depends in part on the spacing of the isopycnals, and so on their steepness in the ACC region. If the mesoscale eddies are not parameterized or are poorly resolved the isopycnals will be too steep and the isopycnals spread too far apart; the mixing and consequently the MOC strength will be too low and the heat uptake into the abyss may be too weak.

3. Model Formulation and Experiment Design

a. Model Set-up

We use the Modular Ocean Model (MOM) version 4 (Griffies et al. 2004) with spherical coordinates and configure it as an idealized representation of the Atlantic Ocean, similar to various studies of the steady state MOC and ocean stratification (Vallis 2000; Nikurashin and Vallis 2011, 2012; Wolfe and Cessi 2010, 2011), the oceanic transient response to changing atmospheric winds

(Jones et al. 2011), and the response of the MOC to changes in wind and buoyancy forcing in an eddy-permitting model (Shakespeare and Hogg 2012). The model domain is an inter-hemispheric basin with 48° zonal width extending from 75°S to 75°N. A 10°-wide zonal channel is opened between 65°-55° in the southern hemisphere to represent the Antarctic Circumpolar Current. There are 36 levels in the vertical over an ocean depth of 4000 m, with layer thickness increasing from 10 m to 300 m. The model ocean is flat-bottomed everywhere, except near the two zonal walls where continental slopes with 8° width extending from about 800 m below the surface to the bottom. We acknowledge that the bathymetry in Drake Passage plays an important role in ACC dynamics itself in particular its zonal transport and larger-scale ocean circulation. Without bottom topography in the latitudes of the open channel, no zonal pressure gradient can be supported and the geostrophic constraint prevents efficient meridional spreading of the flow in the deep ocean, which may lead to excessively weak lower MOC cell and its trapping near the southern boundary (Vallis 2000), especially in the presence of weak eddy effects or strong surface westerlies. However, in the presence of mesoscale eddies the differences in the MOC between flat-bottomed and topographic simulations are much smaller (Henning and Vallis 2005), and so as the first step towards an understanding of the basic dynamics of ocean heat uptake we do not consider any topography in the channel throughout the paper.

We use three versions of the model with the same configuration but different horizontal resolutions: a 2° coarse-resolution model, a 0.25° eddy-permitting model and a 0.125° eddy-resolving model. Momentum is dissipated by horizontal Laplacian viscosity, vertical viscosity, and quadratic bottom drag with coefficients $A_h = 1.0 \times 10^5\,\mathrm{m^2\,s^{-1}}$, $A_v = 1.0 \times 10^{-3}\,\mathrm{m^2\,s^{-1}}$ and $C_d = 1.0 \times 10^{-3}$. In both eddy-permitting and eddy-resolving models, the Laplacian viscosity is replaced with biharmonic friction with a Smagorinsky viscosity (Griffies and Hallberg 2000). The vertical diffusivity, κ, is set constant through the water column. The effects of eddies in the coarse-resolution model is parameterized with a Gent–McWilliams-like scheme, specifically with a vertically non-local eddy-induced transport streamfunction for each ocean column (Ferrari et al. 2010), and the mixing coefficient κ_e is set as $500\,\mathrm{m^2\,s^{-1}}$. No parameterization for sub-grid isopycnal eddy mixing is used

in the two high-resolution models.

We use a linear equation of state and assume salinity is constant and equal to 35 psu; that is, buoyancy is a linear function of temperature. Surface buoyancy forcing Q is given by a relaxation to a fixed temperature profile $T^*(y)$ at the top grid box (Fig. 2b):

$$Q = -\lambda(T_s - T^*), \tag{1}$$

where T_s is the ocean surface temperature and λ is the relaxation coefficient set at $16\,\mathrm{W\,m^2\,K^{-1}}$ corresponding to a restoring time scale of 30 days. The model ocean is also driven at the surface by a latitude-dependent zonal wind stress (Fig. 2a), and its maximum amplitude in the southern ocean is near the equator-ward flank of the channel and is denoted as τ_s. The various simulations discussed in the paper explore the effects two key physical factors, the vertical diffusivity κ, and the Southern Ocean wind τ_s, as well the model resolution and the effects of mesoscale eddies.

b. Experiment design

Multiple sets of runs are carried out with the coarse resolution model. Each set consists of a control climate simulation (CTL henceforth), representing the steady state climate with a distribution of T^* that is the same for all sets, and several warming climate simulations. In CTL, the model is integrated for 4800 years with constant (κ, T^*, τ_s). Starting from year 4000, warming experiments are integrated in which the restoring temperature, T^*, is increased instantly, either regionally or globally with uniform amplitude, and kept fixed for 800 years. The difference between the warming experiment and the final 800 years of CTL is referred to as the change induced by the climate warming. Four experiments with perturbed T^* are considered. In experiments WN (warming at northern high latitudes), WS (warming at southern high latitudes), and WM (warming at low and middle latitudes), regional warming is considered by enhancing the restoring temperature at latitudinal bands of 55°-75°N, 55°-75°S, and 50°S-50°N. The uniform warming case is investigated in experiment W, where T^* is increased everywhere by 2°C.

In our exploration of the basic mechanisms driving ocean heat uptake in Section 4 using a

relatively coarse model, we set $\kappa = 0.5 \times 10^{-5} m^2 s^{-1}$ and $\tau_s = 0.2 N m^{-2}$. The small value of κ corresponds to a nearly adiabatic ocean interior that helps to isolate dynamic processes other than thermal diffusion in driving heat uptake. For the high-resolution runs we describe just one experiment, one with uniform warming denoted W. The vertical diffusivity is now set at the value closer to that in the real ocean, $\kappa = 4 \times 10^{-5} m^2 s^{-1}$ and the southern ocean westerlies is $\tau_s = 0.2 N m^{-2}$. The eddy-permitting model is interpolated from a coarse-resolution model integration with identical (κ, τ_s) and integrated for 500 years, from where the eddy-resolving model is initialized and integrated for an addition 250 years. The warming experiments are carried out in the last 100 years in both models.

The sensitivity of the model ocean to diapynal mixing and Southern Ocean wind is explored by varying κ and τ_s in two sets of runs in the coarse-resolution model. In the first set, τ_s is prescribed at $0.2 N m^{-2}$ while κ is set at 0.1×10^{-5}, 0.5×10^{-5}, 1×10^{-5}, 2×10^{-5}, 3×10^{-5}, 4×10^{-5}, 6×10^{-5}, 10×10^{-5}, and $20\times10^{-5} m^{-2} s^{-1}$. In the second set, τ_s is set at 0.025, 0.05, 0.1, 0.2, 0.3 and $0.4 N m^{-2}$; a slightly low vertical diffusivity ($\kappa = 2 \times 10^{-5} m^2 s^{-1}$) is chosen, so that different water masses in association with upper and lower MOC cell are more distinctive, which makes it easier to discern effects of changing wind stress in affecting each water mass and the associated heat uptake.

In what follows, we will first isolate the different mechanisms of heat uptake using regional warming experiments with the coarse-resolution model, then investigate similarity and difference among models with different resolutions. Finally, the effects of diapycnal diffusivity and Southern Ocean wind on ocean heat uptake are explored with the coarse-resolution model. In figures showing the time evolution of various quantities, the time axis starts at the beginning of the warming experiments rather than the beginning of the control climate simulation.

4. Mechanisms governing ocean heat uptake

a. Equilibrium structure

In equilibrium, the ocean stratification is characterized by three thermoclines that are readily identified as three local maxima of temperature's vertical gradient near the polar end of the subtropical gyre (Figs. 3a and 3b). The near surface maxima of stratification is coincident with isopycnals outcropping in the subtropical gyre, demonstrating the existence of a ventilated thermocline (Luyten et al. 1984) where ocean dynamics can be well described by adiabatic and inviscid assumptions. Below it, an internal thermocline resides in the upper ocean, in conjunction with isopycnals outcropping in both the northern and southern hemisphere (Samelson and Vallis 1997). The deep thermocline, as illustrated by the third local maxima that is related to isopycnals outcropping in the southern hemisphere, is a consequence of the combined effects of the zonal channel and the surface buoyancy gradient across it (Vallis 2000). Corresponding to these three thermoclines are the shallow, upper and lower meridional overturning cells (Fig.3c), as described in Section 2. Water parcels within the temperature range shared between the northern and southern hemisphere are transported along the upper MOC cell essentially adiabatically in ocean interior. Water parcels with even colder temperature are carried along the lower cell counter-clockwise in the meridional plane.

b. Ocean responses in regional warming experiments WM, WN, and WS

Based on ocean responses in the three experiments with regional warming, we can distinguish two distinct processes of ocean heat uptake that are governed by different mechanisms and are significantly different in penetration depth and time scale. With surface warming just in subtropical gyres, as in experiment WM, water parcels with higher temperature leave the ocean surface as pushed down by Ekman pumping and then quasi adiabatically circle along the ventilated thermocline. In the limit of weak diapycnal mixing as in Figs. 4 and 5 where $\kappa = 0.5 \times 10^{-5} m^2 s^{-1}$, downward diffusion of heat across the base of the main thermocline is negligible, so heat is quickly built up within the thermocline till it reaches equilibrium with the surface restoring temperature. The

associated time scale is only a few decades, after which little heat is absorbed into the ocean (the solid line in Fig. 5a). As to the vertical distribution, the magnitude of heat anomaly falls quickly from the surface to nearly zero over about a few hundred meters, leaving the immense deep ocean nearly intact (the solid line in Fig. 5b).

In contrast, under surface warming in high latitudes as in WN and WS, heat is taken up below the main thermocline, in the internal (WN) and deep thermocline (WS), over a time scale of a thousand years (Figs. 4 and 5). Meridionally, It extends beyond the forcing region from high to low latitudes. Although the perturbation of surface buoyancy forcing in the three experiments are of similar magnitudes, changes of ocean heat content in WN and WS far exceed that in WM by the end of the integration. In other words, the ocean is potentially more capable of taking up heat with warming at high latitudes. The driving mechanism is fundamentally related to the upper and lower MOC cells.

Under surface warming in northern high latitudes, temperature of the cold, deep water formed by convection is enhanced. Some isotherms, previously within the upper MOC cell, such as 5°C isotherm, is flattened near the northern boundary and become isolated from the atmosphere (Fig. 6a). No water is convected to them any longer, but in the channel water parcels on these isotherms continue to be sucked to the surface nearly adiabatically. They are subsequently carried northward by the upper limb of MOC, and are finally transferred diabatically to a temperature higher than it has upon arriving at the surface in the channel, due to the surface warming. As a consequence, the volume of the thermostad between temperature 4-5°C declines over time, while the volume of water masses with higher temperatures, such as 6-7°C, is increased (Fig. 6a). Mass is redistributed from cold to warmer water, as shown clearly in Fig. 6b, and the upper MOC cell is warmed up with a peak of temperature change centered around the depth of the maximum strength of MOC (Fig. 5b). A central point for this process is a mismatch between the southern circumpolar channel and the convection region in the northern hemisphere. That is, some isopycnals outcropping in both the channel and the northern hemisphere become isolated from the atmosphere in northern high latitudes due to weakening of convection; water parcels upwelled along these isopycnals

to the surface of the channel are carried northward, and transferred to water masses with higher temperatures than in CTL.

With the surface forcing applied instantly and kept fixed through 800 years, the maximum strength of the MOC falls quickly in a couple of decades (Fig. 7a), and the amplitude of the reduction is proportional to the strength of the surface warming (not shown). This initial reduction is followed by a slow recovery over a few hundred years to a new steady state corresponding to the new T^*. Presumably, the strength of MOC at this new steady state may not be necessarily lower than the CTL value depending on the structure of the new T^*, i.e., its meridional gradient. The strength of MOC within the channel, however, is determined by local isopycnal structures and the westerlies. As isotherms are lowered down in the closed basin, they become steepened in the channel as their outcropping latitudes are mostly fixed at the surface. In the coarse resolution model, the steepening of isotherms in the channel directly leads to the strengthening of eddy-driven isopycnal transport, by GM parameterization, and hence weakening of the upper MOC cell (Fig. 7b). It is found to decline continuously over a time scale of 1000 years till the heat uptake ceases. Affected by these isotherms, isotherms of the lower MOC cell are also steepened in the channel, and the lower MOC cell is strengthened (Fig. 7b).

A cooling tendency is noticed in the lower MOC cell while the upper MOC cell warms up. For example, in Fig. 6a, the 3° and 4° isopycnals are slightly raised up, whereas the 2° ispycnal remains unchanged, suggesting a regional cooling tendency that is also noticeable as a negative bump in the vertical distribution of temperature change (the dashed line in Fig. 5b). This tendency is consistent with changes of water masses, as indicated by Fig. 6b: the volume of water colder than about 3° is increased, along with a reduction of the water volume with temperature between 3 and 4°. One explanation for these shifts is as follows. With the continued weakening of the upper MOC cell, some water parcels previously flowing along the upper MOC cell start to circulate along the lower MOC cell at some point. Then they begin to be carried southward, instead of northward, after being upwelled to the surface in the channel, transferred to lower temperature and convected to depth. This is a process opposite to the process described for warming in the upper MOC cell, and leads to

heat loss to the atmosphere.

Under the surface warming in southern high latitudes (WS), the coldest surface temperature is increased and isotherms ventilated within that zonal band intersect the surface further southward. Along isotherms in the lower MOC cell, cold water upwelled to the surface is warmed and then convected to the abyss. Volume is therefore redistributed from lower to higher temperatures (Fig. 6c). The warming tendency starts from the abyss near the southern boundary and spreads northward along isotherms. Some of the isotherms in the upper MOC cell are also within the heating area, so ocean heat content is also observed to increase in the upper MOC cell as a little bump in the vertical distribution plot (the dash-dot line in Fig. 5b). As isopycnals' outcropping latitudes move southward, the isopycnal slopes become flatter. Correspondingly, the strength of the lower MOC cell is reduced (Fig. 7c).

c. Relation between WM and WN

The heat uptake in the ventilated thermocline and in the deep ocean are also connected due to ocean meridional transport, and is readily seen in the experiment WM of a case with $\kappa = 2 \times 10^{-5} m^2 s^{-1}$ and $\tau_s = 0.2 N m^{-2}$, where the strength of upper MOC is much greater than what is previously discussed due to the enhanced diapycnal diffusion. With higher diapycnal diffusivity, heat can be diffused more effectively across the base of the main thermocline. Meanwhile heat absorbed in tropics and subtropics is carried northward by ocean circulation. Once the surface is warmed up at the northern high latitude convection region, the same process as in WN takes place. This explains why in Fig. 8, heat uptake also occurs below the main thermocline and within the upper MOC cell, extending southward. The total ocean heat content, instead of increasing quickly within about 10 years as in the low diffusivity case (Fig. 5a), increases more slowly over 1000 years as determined by the second mechanism (not shown).

Overall, then, there are two mechanisms driving ocean heat uptake: one that applies to the ventilated thermocline and one that applies to the ocean at mid-depth and in the abyss. Heat enters the ocean through Ekman pumping for the first mechanism. For the latter, water parcels in the deep

ocean are carried to the surface in their circuit along the two MOC cells and are warmed before they are convected to depth. Both the penetration depth and the magnitude of the total heat uptake are much greater in the second process. In all these experiments with regional warming, the amplitude of the perturbation determines the strength of ocean response and heat uptake, so it is very likely that the temperature change at the mid-depth or in the abyssal ocean is larger than that in the upper ocean, in response to a geographic distribution of surface warming with greater amplitude at high latitudes.

5. Responses to uniform warming in low- and high-resolution models

Under the uniform warming, the upper, mid-depth and abyssal ocean take up heat simultaneously through different mechanisms as discussed in Section 4. Temperature changes in low and high-resolution models share the similar pattern (Fig. 9). For example, the amplitude of temperature change fall with depth in the closed basin, but is greater in the abyss near the southern boundary. This is due to the northward and downward extension of heat along the lower MOC cell as in WS (Figs. 4d and 4e). Although the surface buoyancy perturbation is uniform, the ocean heat uptake shows latitudinal dependence: the column inventory is somewhat uniform in low and middle latitudes, but is characterized by a strong warming in the southern channel and weak warming or cooling tendency around the polar edge of the subtropical gyre in the northern hemisphere (Fig. 10a). The horizontally-mean heat uptake is strongest near the surface and declines with depth (Fig. 10b).

The ocean circulation also responds similarly in the three models. The maximum overturning circulation, found in northern high latitudes, first quickly declines and then slowly recovers over a 100-year time scale (Fig. 11a), as in experiment WN discussed in Section 4. However in the channel, the upper MOC cell strengthens, along with the weakening of the lower cell (Figs. 11b and 11c). In the coarse resolution model, these changes of MOC imply the slumping of isopycnals,

caused by their southward migration of outcropping latitudes and leading to the weakening of the parameterized eddy-driven transport, strengthening of upper MOC as well as weakening of the lower MOC. Isopycnal steepness, calculated as $-T_y/T_z$, is also found to decrease in high resolution models over most of the area within the channel (not shown), which is consistent with the coarse-resolution model results.

Despite the similarities, there are two important differences between the models with different resolutions. First, the warming amplitude around 50°N is smallest in the highest resolution model and biggest in the coarse resolution model. This is noticeable in Fig. 9 and is more remarkable in the latitudinal distribution of temperature change (Fig. 10a). Second, warming near the southern boundary and in the abyssal ocean is very weak in the eddy-permitting model, much weaker than the coarse-resolution and eddy-resolving model (Figs. 9 and 10). The rest of the section will focus on these two issues.

It is important to remember that neither the 0.25° nor the 0.125° model uses any parameterization scheme for effects of sub-grid-scale eddies, and whether eddy effects can be sufficiently resolved is critical for dynamics within the southern channel where the eddy-driven meridional transport has an order one influence on the dynamics by counteracting the mean forced by the westerlies. The vertically and zonally integrated eddy heat flux, $[\overline{V'T'}]$ can be regarded as a measure of strength of eddy effects, and is calculated as the difference between the total advective flux $[\overline{VT}]$ and the flux by the mean flow $[\bar{V}\bar{T}]$:

$$[\overline{VT}] = \int_{-h}^{0} dz \int_{x_w}^{x_e} dx \overline{V(x,y,z,t)T(x,y,z,t)}, \tag{2}$$

$$[\bar{V}\bar{T}] = \int_{-h}^{0} dz \int_{x_w}^{x_e} dx \overline{V(x,y,z,t)} \quad \overline{T(x,y,z,t)}, \tag{3}$$

where bars denote the average over the last 10 years, $-h$ is the value of z at the ocean bottom, x_w and x_e denote locations of the western and eastern boundaries. Figure 12 shows eddy heat fluxes of the two high resolution models in CTL (panel a) and their changes in experiment W (panel b). To have a better comparison of the role of eddies role in the two models, the eddy-driven heat flux in each model is normalized by the maximum strength of the total heat flux over all latitudes. In

both models, the eddy contribution is negligible compared with the mean flow except within the channel where the two have comparable strength with opposite signs. In comparison with the 0.25° model, the 0.125° model has a much greater contribution from eddies both within and out of the channel. The stronger southward eddy transport in the channel is more powerful in slumping the isopycnals down, raising isopycnals in the closed basin by as much as 500 m from their levels in the 0.25° model (Fig. 13). Consequently, the lower MOC cell spans a greater depth range with greater amplitude in the model with the highest resolution (Fig. 14). Under surface warming in the southern high latitudes, stronger circulation along the lower MOC cell means water parcels in the abyss are more quickly brought upward to the surface to be warmed, causing stronger warming tendency in the lower MOC cell near the ocean bottom.

Under the uniform warming, the eddy-driven heat flux is found to be weakened in most of the area within the channel with greater reduction in the 0.125° model, consistent with the slumping of isopycnals, strengthening of the upper MOC cell and weakening of the lower MOC cell (Figs. 11b and 11c).

Though the feature of excessively low warming amplitude (or a strong cooling tendency) around 50°N near the ocean surface is absent in the coarse resolution model between year 90-100 (Fig. 9a), it is remarkable in the experiment WN where the surface warming is only applied at northern high latitudes (Fig. 4c). It is also one of the most obvious features in ocean response to warming climate in both a simplified ocean circulation model (Xie and Vallis 2011) and a more complicated atmosphere-ocean-ice coupled model (Stouffer et al. 2006b). As suggested by Xie and Vallis (2011), redistribution of existing heat reservoir by ocean circulation change is the main contributor to this cooling tendency. As shown in Fig. 15a, under the surface warming, the northward meridional heat transport in the northern hemisphere is reduced, presumably resulting from the weakening of the upper MOC cell. This reduction strengthens significantly from low- to high-resolution models, consistent with Fig. 15b where the reduction of MOC averaged between 40 °-50° N is stronger in the high-resolution model except during the first 20 years. It demonstrates the causal relation between the MOC reduction and the near surface cooling in northern high latitude.

Overall, the coarse- and the two high-resolution models generate qualitatively similar results of ocean heat uptake and ocean circulation changes under the uniform warming. The change of the ocean's total heat content within 100 years in the three models differ by less than 12%, owning mostly to the difference of the lower MOC cell. Because of the stronger eddy effects, the 0.125° model has the strongest lower MOC cell and hence largest change of ocean heat content. It also has the most significant changes of ocean circulation and eddy heat flux. The eddy-permitting model, in the absence of any parameterization scheme for eddy mixing, has insufficient eddy flux to counter wind-driven mean circulation in the circumpolar channel, leading to steeper isopycnals and weaker lower MOC cell.

6. Effects of Diapycnal mixing and Southern Ocean wind

a. The equilibrium state

The diapycnal mixing and westerlies in the southern circumpolar channel are essential for maintaining the overturning circulation and deep stratification in the ocean (Vallis 2000; Nikurashin and Vallis 2012). Since 1970s, the winds over the Southern Ocean have been undergoing a poleward intensification (Thompson and Solomon 2002), and it has been suggested that such shifts may have significant impacts on ocean heat and carbon uptake (Russell et al. 2006; Fyfe et al. 2007). In this section, the effects of the southern ocean wind and diapycnal mixing will be investigated with our idealized ocean model.

Before trying to understand the sensitivity of the transient response to κ and τ_s, we first look at their influence on the equilibrium state. Diapycnal mixing offers one mechanism, albeit a weak one given the magnitude of diffusivity in the present climate ocean, governed by the advective-diffusive balance, to raise the cold water in the ocean interior and balance sinking at high latitude convection regions. In the limit of weak diffusivity, the three thermoclines are well separated by two thermostads with fairly large volume and very weak stratification (Fig. 16a). As κ increases, boundaries of those thermoclines become ambiguous (Fig. 16b) and the maximum stratification

declines for both MOC cells (Fig. 16c). All isopycnals are brought down in the closed basin and the deep ocean is filled with water of higher temperature. The upper MOC cell expands in both depth and temperature range; the lower MOC cell is squeezed, not as much as the expansion of the upper cell, leading to a reduction of the volume of the thermostad between the two cells (Fig. 16b).

In the circumpolar channel, the westerlies provide another route for the upwelling leg of MOC: cold, deep water is upwelled adiabatically along isopycnals by convergence. They exert a strong influence on the rate of MOC and deep stratification by pushing down isopycnals in the channel. With stronger westerlies, the deep ocean also becomes warmer, similar to the response to increasing κ. A major difference between changing κ and changing τ_s is the former is a global effect at all levels, whereas the latter acts on part of isopycnals. Although both MOC cells have isopycnals outcropping in the channel, the effects of changing wind on them may differ in strength depending on the actual meridional structure of τ_s. In Fig. 17c, the downward expansion of the upper MOC cell is not as remarkable as for changing κ. In some contrast, the lower MOC cell is strongly affected: as isopycnals are made more steeper under strong wind, the lower MOC cell is lowered down and squeezed in the depth range. When τ_s is twice the magnitude used in the reference case, the lower MOC cell only exists in a small region near the southern boundary, causing the thermostad between the two MOC cells to expand in size (Figs. 17a and 17b).

Based on our understanding of the driving mechanism for deep ocean heat uptake in the reference case and the comparison among models with different resolutions, we believe the strength of MOC is a key factor determining the magnitude of heat absorption in the ocean. We find similar parameter dependence of MOC rates to previous analytical and modeling studies (Nikurashin and Vallis 2011, 2012; Shakespeare and Hogg 2012). The rate of the upper MOC, as usually defined as the maximum overturning streamfunction, increases with both κ and τ_s (Figs. 18a and 18c, circles). The rate of the lower MOC cell, defined as the mean lower cell overturning streamfunction outside the channel, increases with κ but changes inversely with the southern ocean wind (Figs. 18b and 18d, circles).

Inspired by the fact that the strength of MOC within the channel is more closely related to the heat uptake process in WN and its evolution is different from that of the maximum strength of MOC,

we also investigated MOC within the channel. Interestingly, the rate of the upper MOC cell within the channel declines with increasing κ (Fig. 18a, squares), opposite to the changing tendency of the *maximum* MOC strength. Moreover, under strengthening wind, the strength of the lower MOC in the channel first decreases in the low τ_s regime and increases in the medium to strong wind regime (Fig. 18d, squares).

b. The response to regional warming

To find out how the eddy diffusivity and southern ocean westerlies affect the ocean heat uptake, changes of heat content in warming experiments with different κ or τ_s are compared side by side for the entire integration period (800 years). For most cases, and unless otherwise stated, choosing a different time for comparison (for example up to year 400 instead of 800) does not lead to qualitatively different results.

Let us first look at dependence of ocean heat uptake on κ and τ_s in regional warming experiments. As shown in Figs. 16c and 17c, changing κ or τ_s does not have strong effects on the depth of the ventilated thermocline, which is about 150 m below the surface. The heat anomaly above this level under low- and mid-latitude warming is also insensitive to changing parameters (Figs. 19a and 20a, circles). This insensitivity is a manifestation of the fact that the ventilated thermocline is mostly controlled by the wind in subtropical gyres and its dynamics is nearly adiabatic and inviscid. At low diffusion limit, all the heat absorbed by the ocean is contained within the ventilated thermocline, but as diffusion becomes stronger, heat enters the deep ocean through diffusion across the base of the thermocline. Meanwhile, it is taken up by the same process discussed for WN after surface water in northern high latitudes is warmed by anomalous heat transported from low latitudes. The strength of this process is strongly affected by how much the ocean surface in high latitude region is warmed, which is influenced by the rate of the upper MOC cell in the northern hemisphere. Therefore, although the anomalous heat contained in the surface ocean remains nearly constant, the heat absorbed in the deep ocean increases greatly with the diffusivity (Fig. 19a, squares). Similar pattern is found for changing τ_s: the surface ocean heat uptake is more or less constant, but the deep

ocean takes up more heat under stronger wind that greatly enhances the rate of the upper MOC cell (Fig. 20a, squares).

In experiments with northern high latitude warming, variations of the ocean heat uptake with changing parameters are found consistent with those of the upper MOC's strength in the channel but not in the northern hemisphere convection region. The heat uptake and the rate of the upper MOC cell in the channel remain at about the same level in very small κ regime, but decline for bigger κ (Fig. 19b and Fig. 18a, squares). With increasing southern ocean wind, the uptake increases for low to medium value of τ_s, and then stays constant for strong wind, again similar to the variation of MOC in the channel (Fig. 20b and Fig. 18c, squares). This is not a surprising result and is actually consistent with our understanding of WN in the reference case. As described in Section 4, the heat uptake with warming in northern high latitudes is due to a mismatch between the temperature of water formed in convection region and the temperature of water upwelled in the channel. After water parcels being pumped into the surface in the channel, they are transported northward, transferred to a warmer temperature upon arriving at the convection site. It is critical, as they are transported northward, to remain near or at the surface in order to obtain heat from the atmosphere through air-sea interactions. In addition to this 'surface' route along which water returns to the convection site, there is an 'interior' route where water parcels upwell across isopycnals through the advective-diffusive balance. The latter makes no or little direct contribution to heat absorption from the atmosphere since water parcels on this route are rarely ventilated. The maximum strength of the upper MOC is determined by both routes, therefore its variation is not closely tied to the heat uptake in WN.

For warming in southern high latitudes, the situation is a little complicated because not only the isotherms within the lower MOC cell, some isotherms in the upper MOC cell also outcrop in the warming area. Therefore, heat is built up in the lower as well as the upper MOC cell, although with a lower rate. Defining the lower MOC cell as the volume consisting of water parcels with temperature lower than the coldest temperature in the northern hemisphere in CTL, we calculated its heat uptake during the first 100 years, to avoid as little as possible heat built up in the upper

MOC cell, and found similar variation tendency to the rate of the lower MOC cell in the channel (Figs. 19c and 18b, Figs. 20c and 18d, squares). Although under strong wind such as $\tau_s = 0.4Nm^{-2}$, isopycnals in association with the lower MOC cell are very steep and the lower MOC cell has a relatively narrow meridional range, the heat absorption in the southern ocean is strong due to strong lower MOC circulation in the channel. Although in our simulations the surface wind stress is constant for both control and warming climate simulations, it is presumably true that in response to transient, strengthening westerlies, the southern ocean heat uptake is also intensified due to the strengthening of the lower MOC cell in the channel, which is consistent with evaluations made by Russell et al. (2006).

c. On responses to uniform warming

Responses to uniform warming is the combined effects of different driving mechanisms of heat uptake. The heat uptake strengthens with increasing parameters except in the experiment WN where it has a declining tendency with increasing κ. This tendency for decrease can be easily overwhelmed by the tendency for increase in response to warming in the subtropics and in the southern ocean. Therefore, it is not surprising to see the heat content change under the uniform warming increases with both parameters. With increasing κ, the heat uptake stays around the same level in regime of very low diffusivity, and scales as $\kappa^{1/3}$ for larger diffusivity (Fig. 21c). With strengthening southern ocean wind, the heat uptake increases and scales with τ_s as $\tau_s^{1/2}$ (Fig. 22c). The change of heat content integrated through the whole water column increases with both parameters in all latitudes, with a much greater increasing rate in the southern ocean (Figs. 21a and 22a). As discussed in experiments with regional warming, the heat absorbed in the ventilated thermocline is quite insensitive to both parameters. The total heat absorption declines with depth, but the vertical gradient is reduced with increasing parameters (Figs. 21b and 22b).

7. Discussion and Conclusions

In this paper, we have identified two distinct mechanisms driving heat uptake in the ocean in response to an enhanced surface restore temperature. One is heat uptake into the ventilated thermocline driven by Ekman pumping in the subtropical region, and the other is heat uptake in the upper and lower MOC cells. The temperature increase by the first mechanism occurs in the thermocline over a time scale of a few decades, whereas that by the second mechanism occurs mostly at mid-depth and in the abyssal ocean over a time scale of centuries to millennia. The magnitude of heat uptake in the ventilated thermocline by the first mechanism is largely insensitive to the southern ocean westerlies and diapycnal mixing, while that by the second mechanism in the upper (lower) MOC cell is largely determined by the rate of the upper (lower) MOC cell in the channel, and hence is affected by both winds and mixing. In the case of warming with a spatially uniform amplitude, both mechanisms occur simultaneously and the resulting ocean heat uptake increases with both winds and mixing. In particular, the southern ocean takes up more heat when there are stronger westerlies.

Eddy processes in the channel are essential for the production of deep stratification and overturning circulation of the entire ocean, but they are not sufficiently resolved in the 0.25°, eddy-permitting model. The weak eddy transport in the eddy-permitting model leads to steeper isopycnals, a deeper upper MOC cell, and a very weak lower MOC cell in the control climate (consistent with the theory of Nikurashin and Vallis 2012). As a result, the heat uptake in the abyssal ocean is much weaker in the eddy-permitting model than in the eddy resolving model. The ocean circulation changes in response to the uniform warming are of the same sign in both eddy-permitting and eddy-resolving models, with eddy transfer in the channel weakening owning to the slumping isopycnals driven by the surface warming, but the amplitude of the change is much greater in the eddy-resolving model. One consequence of this is that as coupled climate models move into an ocean-eddy permitting regime, care will evidently have to be taken when interpreting the results of ocean heat uptake.

Owing to the very idealized model configurations adopted in the study, there are some potential limitations for its application to the real ocean. One is that the surface boundary condition for

buoyancy in our experiments is a relaxation to a prescribed temperature whereas in the real ocean it is more complicated, with aspects of both a fixed-buoyancy-flux and a relaxation. With a fixed buoyancy flux at the surface the water-mass transformation rate within the mixed layer might be hard to change and the MOC might then be less sensitive to property changes in ocean interior, and some of our results might not hold as cleanly. Perhaps a more severe limitation is that in our study the buoyancy is only a function of temperature and we have neglected both saline and ice processes. Thus we are unable to separate the effects of salinity change and that of temperature change. Finally, our domain is very idealized and we have sidestepped the geographical and bathymetric complexity of the real ocean. In particular we have not include any bottom topography across the circumpolar channel, and this certainly will affect the strength of the ACC and, to a lesser extent, the strength and extent of the lower MOC cell and therefore heat uptake into the abyss.

Nevertheless, there is evidence for consistency between reality and our model simulations. For example, a recent observational study found a significant reduction in the AABW volume between 1980s and 2000s, along with the descent of potential isotherms and heat uptake in both AABW and the entire ocean (Purkey and Johnson 2012). It was believed that this bottom water contraction was consistent with the reduction of the AABW formation rate and the slowing down of the bottom, southern limb of MOC, probably induced by the freshening of shelf waters in AABW formation regions in the Ross and Weddell Seas in recent decades (Aoki et al. 2005; Jacobs and Giulivi 2010; Hellmer et al. 2011). Similarly in our numerical simulations, in response to surface warming either only in the southern channel or in the global scale, the lower MOC cell in the channel slows down, along with the lowering of the associated isotherms. Therefore, idealized models, as the one used in the present study, though lack many probably relevant features as listed above, is a valuable tool in attempting to understand and predict ocean response to climate change.

Acknowledgments.

We would thank two anonymous reviewers for remarks that significantly improved this paper. We also thank Isaac Held for useful comments, Maxim Nikurashin for discussions, and Steve

565 Griffies and Matthew Harrison for their help on the use of MOM. The work was funded by the
566 DOE-SC0005189.

REFERENCES

Andrews, D. G. and M. E. McIntyre, 1976: Planetary waves in horizontal and vertical shear: the generalized Eliassen-Palm relation and the mean zonal acceleration. *J. Atmos. Sci.*, **33**, 2031–2048.

Aoki, S., S. R. Rintoul, S. Ushio, S. Watanabe, and N. L. Bindoff, 2005: Freshening of the Adélie Land Bottom Water near 140^{o}E. *Geophys. Res. Lett.*, **32**, doi:10.1029/2005GL024246.

Banks, H. T. and J. M. Gregory, 2006: Mechanisms of ocean heat uptake in a coupled climate model and the implications for tracer based predictions of ocean heat uptake. *Geophys. Res. Lett.*, **33**, doi:10.1029/2005GL025352.

Bitz, C. M., P. R. Gent, R. A. Woodgate, M. M. Holland, and R. Lindsay, 2006: The influence of sea ice on ocean heat uptake in response to increasing CO_2. *J. Clim.*, **19**, 2437–2450.

Bryden, H. L., H. R. Longworth, and S. A. Cunningham, 2005: Slowing of the Atlantic meridional overturning circulation at 25^{o}N. *Nature*, **438**, 655–657.

Ferrari, R., S. M. Griffies, A. J. G. Nurser, and G. K. Vallis, 2010: A boundary-value problem for the parameterized mesoscale eddy transport. *Ocean Modelling*, **32**, 143–156.

Fyfe, J. C., O. A. Saenko, K. Zickfeld, M. Eby, and A. J. Weaver, 2007: The role of poleward-intensifying winds on Southern Ocean warming. *J. Clim.*, **20**, 5391–5400.

Gnanadesikan, A., 1999: A simple predictive model for the structure of the oceanic pycnocline. *Science*, 2077–2079.

Gregory, J. M., 2000: Vertical heat transport in the ocean and their effect on time-dependent climate change. *Climate Dyn.*, **16**, 501–515.

589 Gregory, J. M. et al., 2005: A model intercomparison of changes in the Atlantic thermohaline
590 circulation in response to increasing atmospheric CO_2 concentration. *Geophys. Res. Lett.*, **32**,
591 doi:10.1029/2005GL023209.

592 Griffies, S. M. and R. W. Hallberg, 2000: Biharmonic friction with a Smagorinsky-like viscosity for
593 use in large-scale eddy-permitting ocean models. *Mon. Wea. Rev.*, **128**, 2935–2946.

594 Griffies, S. M., M. J. Harrison, R. C. Pacanowski, and A. Rosati, 2004: *A technical guide to MOM4*.
595 Ocean Group Tech. Rep., 337 pp.

596 Hellmer, H., O. Huhn, D. Gomis, and R. Timmermann, 2011: On the freshening of the northwestern
597 Weddell Sea continental shelf. *Ocean Sci.*, **7**, 305–316.

598 Henning, C. C. and G. K. Vallis, 2005: The effects of mesoscale eddies on the stratification and
599 transport of an ocean with a circumpolar channel. *J. Phys. Oceanogr.*, **35**, 880–896.

600 Huang, B., P. H. Stone, and A. P. Sokolov, 2003: Ocean heat uptake in transient climate change:
601 mechanisms and uncertainty due to subgrid-scale eddy mixing. *J. Clim.*, **16**, 3344–3356.

602 Jacobs, S. S. and C. F. Giulivi, 2010: Large multi-decadal salinity trends near the Pacific-Antarctic
603 continental margin. *J. Climate*, **23**, 4508–4524.

604 Jones, D. C., T. Ito, and N. S. Lovenduski, 2011: The transient response of the Southern Ocean
605 pycnocline to changing atmospheric winds. *Geophys. Res. Lett.*, **38**, doi:10.1029/2011GL048145.

606 Levitus, S., J. Antonov, and T. Boyer, 2005: Warming of the world ocean, 1995-2003. *Geophys.*
607 *Res. Lett.*, **32**, doi:10.1029/2004GL021592.

608 Levitus, S., J. Antonov, T. Boyer, and C. Stephens, 2000: Warming of the world ocean. *Science*,
609 **287**, 2225–2229.

610 Lumpkin, R. and K. Speer, 2007: Global ocean meridional overturning. *J. Phys. Oceanogr*, **37**,
611 2550–2562.

612 Luyten, J. J., J. Pedlosky, and H. Stommel, 1984: The ventilated thermocline. *J. Phys. Oceanogr*,
613 **13**, 292–309.

614 Marshall, J. and F. Schott, 1999: Open-ocean convection: observations, theory, and models. *Rev.*
615 *Geophys.*, 1–64.

616 Nikurashin, M. and G. Vallis, 2011: A theory of deep stratification and overturning circulation in
617 the ocean. *J. Phys. Oceanogr.*, **41**, 485–502.

618 Nikurashin, M. and G. Vallis, 2012: A theory of the interhemispheric meridional overturning
619 circulation and associated stratification. *J. Phys. Oceanogr.*, **42**, 1652–1667.

620 Purkey, S. G. and G. C. Johnson, 2012: Global contraction of Antarctic Bottom Water between
621 1980s and 2000s. *J. Climate*, **25**, 5830–5844.

622 Radko, T. and J. Marshall, 2006: The Antarctic Circumpolar Current in three dimensions. *J. Phys.*
623 *Oceanogr.*, **36**, 651–669.

624 Röuhlemann, C., S. Mulitza, G. Lohmann, A. Paul, M. Prange, and G. Wefer, 2004: Intermediate
625 depth warming in the tropical Atlantic related to weakened thermohaline circulation: combining
626 paleoclimate data and modeling results for the last deglaciation. *Paleoceanography*, **19**, doi:
627 10.1029/2003PA000948.

628 Rugenstein, M. A. A., M. Winton, R. J. Stouffer, S. M. Griffies, and R. Hallberg, 2013: Northern
629 high latitude heat budget decomposition and transient warming. *J. Climate*, **26**, 609–621.

630 Russell, J. L., K. W. Dixon, A. Gnanadesikan, R. J. Stouffer, and J. R. Toggweiler, 2006: The
631 Southern Hemisphere westerlies in a warming world: Propping open the door to the deep ocean.
632 *J. Clim.*, **19**, 6382–6390.

633 Samelson, R. and G. K. Vallis, 1997: Large-scale circulation with small diapycnal diffusivity: the
634 two thermocline limit. *J. Marine Res.*, **55**, 1–54.

635 Shakespeare, C. J. and A. M. Hogg, 2012: An analytical model of the response of the meridional
636 overturning circulation to changes in wind and buoyancy forcing. *J. Phys. Oceanogr.*, **42**, 1270–
637 1287.

638 Spall, M. A., 2004: Boundary currents and watermass transformation in marginal seas. *J. Phys.*
639 *Oceanogr.*, **34**, 1197–1213.

640 Speer, K., S. R. Rintoul, and B. Sloyan, 2000: The diabatic Deacon cell. *J. Phys. Oceanogr.*, **30**,
641 3212–3222.

642 Stouffer, R. J. et al., 2006a: GFDL's CM2 global coupled climate models. Part IV: idealized climate
643 response. *J. Clim.*, **19**, 723–740.

644 Stouffer, R. J. et al., 2006b: Investigating the causes of the response of the thermohaline circulation
645 to past and future climate changes. *J. Clim.*, **19**, 1365–1387.

646 Thompson, D. W. J. and S. Solomon, 2002: Interpretation of recent Southern Hemisphere climate
647 change. *Science*, **296**, 895–899.

648 Vallis, G. K., 2000: Large-scale circulation and preduction of stratification: effects of wind,
649 geometry, and diffusion. *J. Phys. Oceanogr.*, **30**, 933–954.

650 Visbeck, M., J. Marshall, T. Haine, and M. Spall, 1997: Specification of eddy transfer coefficients
651 in coarse-resolution ocean circulation models. *J. Phys. Oceanogr.*, **27**, 381–402.

652 Wolfe, C. L. and P. Cessi, 2010: What sets the mid-depth stratification in eddying ocean models. *J.*
653 *Phys. Oceanogr*, **40**, 1520–1538.

654 Wolfe, C. L. and P. Cessi, 2011: The adiabatic pole-to-pole overturning circulation. *J. Phys.*
655 *Oceanogr*, **41**, 1795–1810.

656 Xie, P. and G. K. Vallis, 2011: The passive and active nature of ocean heat uptake in idealized
657 climate change experiments. *Clim. Dyn.*, doi:10.1007/s00382-011-1063-8.

List of Figures

7 **(a)** Change of the strength of the upper meridional overturning circulation (ΔUMOC), defined as the maximum meridioal overturning streamfunction in density space, in WN. **(b)** black line: the upper meridional overturning streamfunction (UMOC) averaged within the channel and in the temperature range of 4-5°C in WN; red line: the lower meridional overturning circulation (LMOC) averaged within the channel and below temperature 4°C in WN. Positive value means clockwise circulation, and negative value means counter-clockwise circulation. **(c)** decline of the strength (absolute value) of the lower meridional overturning circulation (ΔLMOC) averaged below temperature 4°C and north of 48°S in WS. This is for the case with $\kappa = 0.5 \times 10^{-5} m^{-2} s^{-1}$ and $\tau_s = 0.2 N m^{-2}$. In WN, the upper MOC cell and the lower MOC cell have continued decline and increase in the channel. In WS, the lower MOC cell is reduced as a consequence of slumping isopycnals. All data are 5-year running average. 40

8 Contours of temperature change in WM at year 400. Under the warming in low- and mid-latitudes, the mid-depth ocean in conjunction with the upper MOC cell warms up slowly and heat extends southward from northern high latitudes. Contour intervals are 0.5°C above 5 and below -5°C, and 0.01°C in between. 41

9 Change of the zonal mean temperature averaged between year 90-100 in W in the coarse resolution run (**a**), 0.25° run (**b**) and 0.125° run (**c**). 42

10 Latitudinal (**a**) and vertical distribution (**b**) of temperature change averaged between year 90-100 in W in the coarse resolution run (dashed), 0.25° run (solid) and 0.125° run (thick solid). It is noticeable in **a** that the southern high latitude warming is weaker in the eddy-permitting model than in the eddy-resolution model, and the cooling tendency near the polar edge of the subtropical gyre is strongest in the eddy-resolving model. In **b**, the change of heat content is stronger in the abyssal ocean in the eddy-resolving model. 43

15 **a** Change of the total meridional heat transport normalized by its maximum value over all latitudes between year 90-100 in W in the coarse resolution (dashed), eddy-permitting (solid) and eddy-resolving (thick solid) model. **b** Change of the meridional overturning circulation in the coarse resolution (dashed), eddy-permitting (solid) and eddy-resolving (thick solid) model in W. The MOC sterngth is defined as the maximum overturning streamfunction below 10 ° C at each latitude and averaged beween 40°-50° N. The result is then normalized by its time-mean strength in the control climate. 48

16 Zonal and time mean temperature in CTL for $\kappa = 0.1 \times 10^{-5} m^2 s^{-1}$ (**a**) and $6 \times 10^{-5} m^2 s^{-1}$ (**b**). **(c)** vertical gradients of mean temperature for κ =0.5×10^{-5} (thick solid), 2×10^{-5}, 4×10^{-5}, and $10^{-4} m^2 s^{-1}$. The maximum vertical gradient declines with increasing κ. 49

17 Zonal and time mean temperature in CTL for $\tau_s = 0.025$ (**a**) and $0.4 N m^{-2}$ (**b**). **(c)** vertical gradients of mean temperature for τ_s =0.05(thick solid), 0.2, 0.3, and $0.4 N m^{-2}$. The maximum vertical gradient declines with increasing τ_s. 50

18 Meridional overturning circulation in CTL. The rate of the upper meridional overturning circulation in the northern hemisphere (circles) and in the channel (squares) for different κ (**a**) and different τ_s (**c**). The rate of the lower meridional overturning circulation in the northern hemisphere (circles) and in the channel (squares) for different κ (**b**) and different τ_s (**d**). 51

19 **(a)** Change of ocean heat content in WM for the entire depth (squares) and above 150 m (circles) at year 800. **(b)** change of ocean heat content in WN at year 800. **(c)** change of ocean heat content in the lower MOC cell in WS and CTL at year 100. Ocean heat uptake at year 100 instead of year 800 is taken for WS in order to have minimum warming within the upper MOC cell. 52

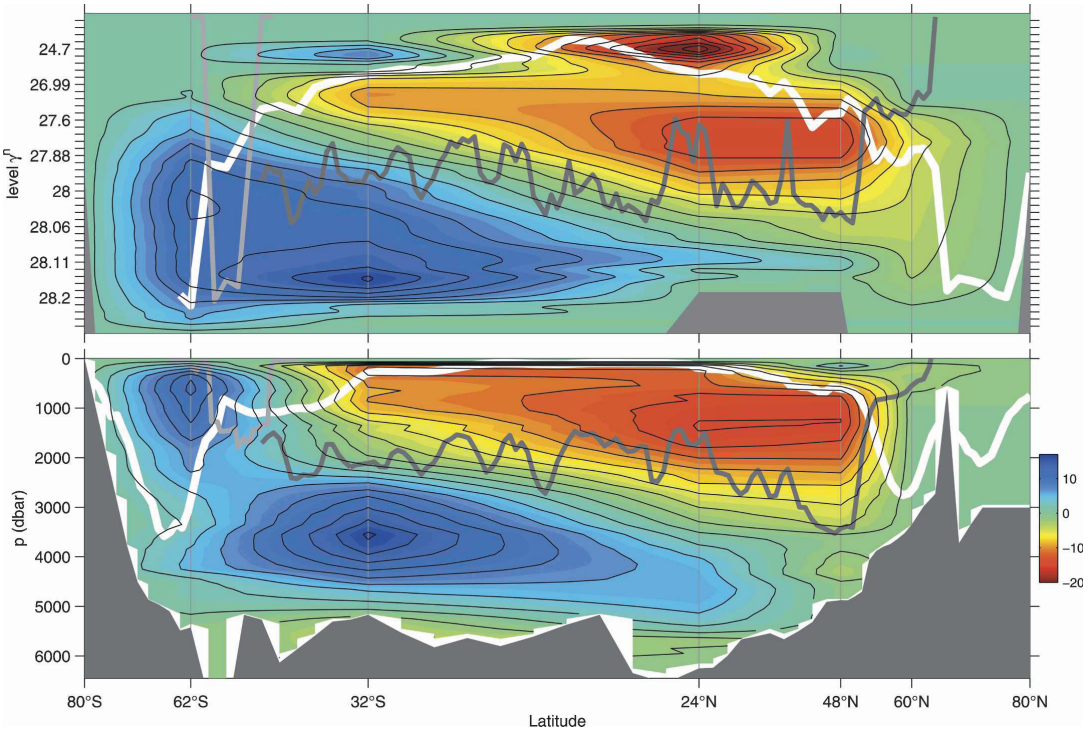

FIG. 1. Zonally averaged global overturning streamfunction in units of Sv and with contour interval of 2 Sv (1 Sv=$10^6 m^3 s^{-1}$) in (top) density and (bottom) pressure coordinates across hydrographic sections (vertical gray lines) with linear interpolation between the sections. Typical winter mixed layer densities/depths (white lines), the mean depth of ocean ridge crests (dark gray lines), and the depth of the Scotia Arc east of Drake Passage (light gray lines) are also shown. From Lumpkin and Speer (2007).

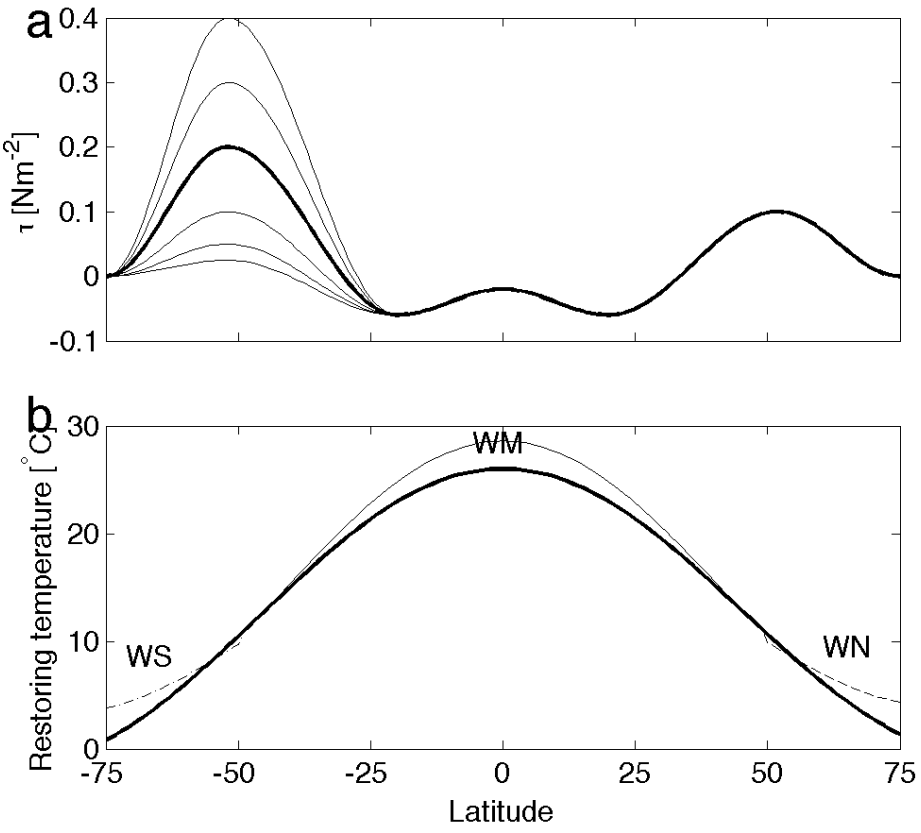

FIG. 2. **(a)** Surface wind stress profile in the reference case with $\tau_s = 0.2Nm^{-2}$ (thick solid line) and in different sets for $\tau_s = 0.0025, 0.05, 0.1, 0.3, 0.4Nm^{-2}$. **(b)** profiles of surface restore temperature T^* used in CTL (thick solid line) of all sets of runs. The thin dashed line denotes the restore temperature in experiment WN that differs from CTL only in northern high latitudes; the thin solid line depicts the restore temperature in WM that is enhanced from CTL in mid- and low latitudes; the thin dash-dot line depicts the restore temperature in WS that differs from CTL only in southern high latitudes. In experiment W, T^* is increased uniformly by 2°C (not shown).

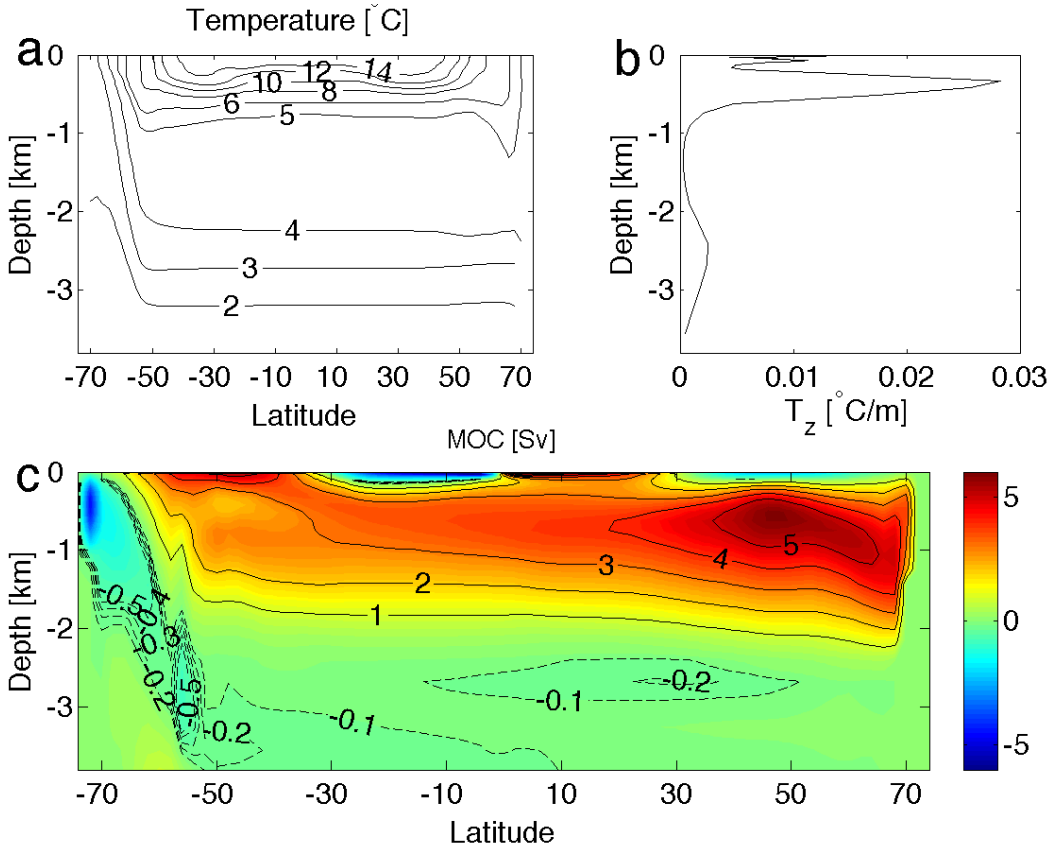

FIG. 3. CTL for the case with $\kappa = 0.5 \times 10^{-5} m^2 s^{-1}$ and $\tau_s = 0.2 N m^{-2}$. **(a)** contours of zonal and time mean temperature. **(b)**, time and zonal mean vertical temperature gradient near the polar end of the subtropical gyre. Three thermoclines are obvious from the temperature derivative plot. In addition to the ventilated thermocline, there is an internal thermocline and a deep thermocline corresponding respectively to the upper and lower MOC cell. **(c)**, meridional overturning streamfunction, as the sum of the mean and the eddy-driven components, $\psi = \bar{\psi} + \psi^*$, in depth coordinates. Solid contours denote values between 1Sv (1 Sv = $10^6 m^3 s^{-1}$) and 5Sv with interval of 1Sv, and dashed contours have values between -0.5Sv and -0.1Sv with interval of 0.1Sv. The strength of lower MOC cell is much weaker than that of the upper MOC cell at this low diffusion limit.

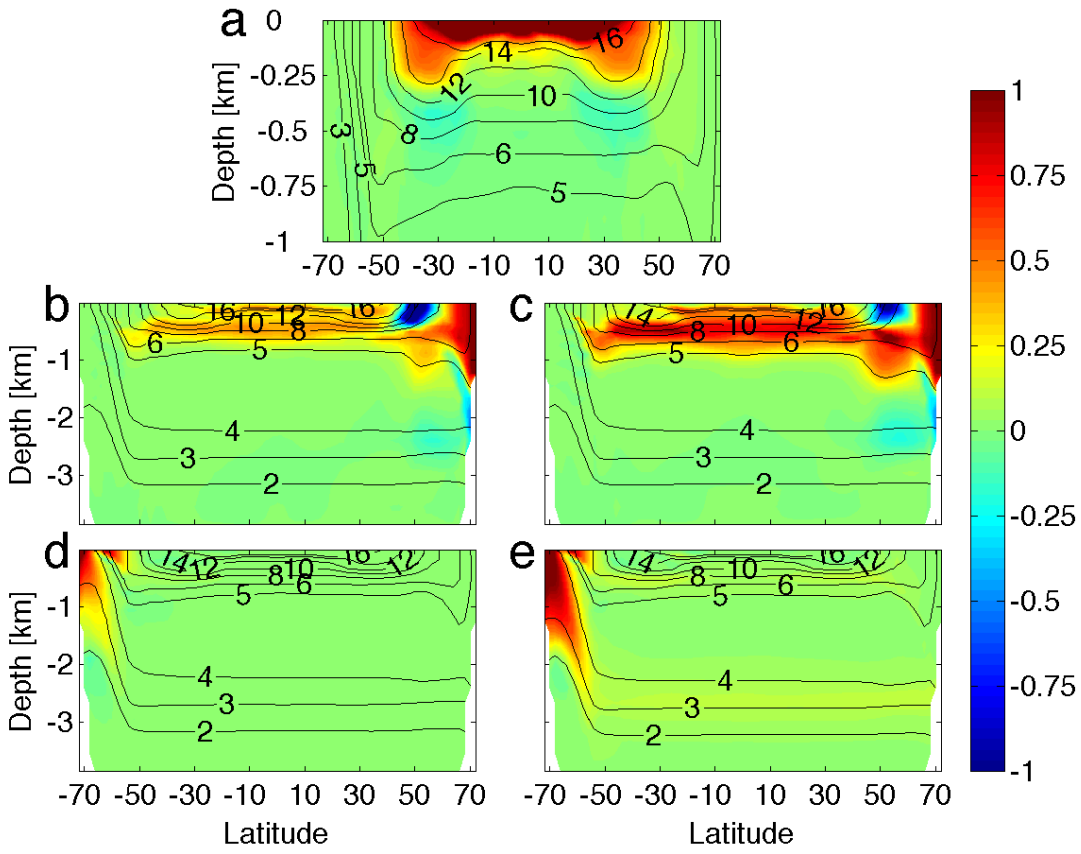

FIG. 4. Temperature change in WM at year 25 (**a**), in WN at year 25 (**b**) and year 50 (**c**), and in WS at year 50 (**d**) and year 400 (**e**). In all experiments, $\kappa = 0.5 \times 10^{-5} m^2 s^{-1}$ and $\tau_s = 0.2 N m^{-2}$. The 'change' is referred to as the difference between the experiment and CTL in the final 800 years of the integration. Clearly, the penetration depth of ocean heat uptake increases in the three experiments, as surface warming at different regions initializes different driving mechanisms. Please note that our time axis starts at the beginning of warming experiments.

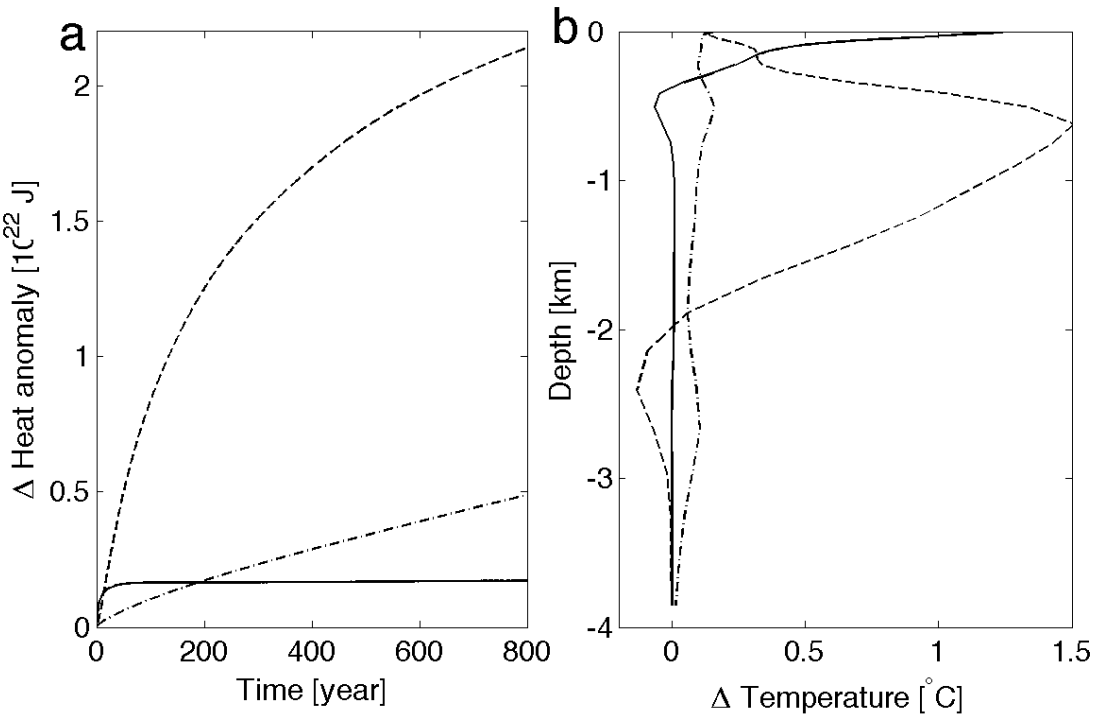

FIG. 5. **(a)** Change of ocean heat content in WM (solid), WN (dashed), and WS (dash-dot) . **(b)** vertical distribution of temperature change in WM (solid), WN (dashed) and WS (dash-dot) at year 400. All experiments are for the case with $\kappa = 0.5 \times 10^{-5} m^2 s^{-1}$ and $\tau_s = 0.2 N m^{-2}$. Ocean takes up heat over quite different time scales in the three experiments. In WM, the heat uptake is concentrated near the surface, while in WN and WS, heat is accumulated at mid-depth and in the abyss.

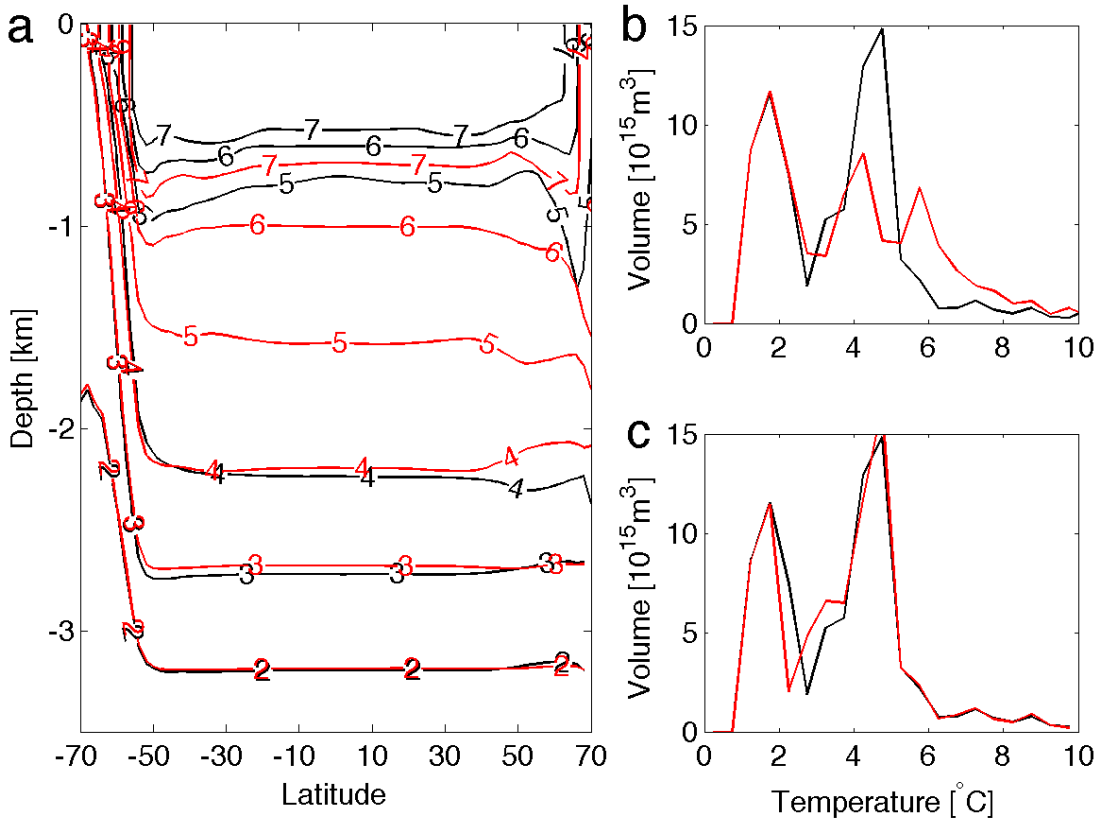

FIG. 6. **(a)** Annual and zonal mean temperature at year 400 in CTL (black) and WN (red). Volumes of water masses versus temperature at CTL (black) and year 400 (red) of experiment WN (**b**) and WS (**c**).

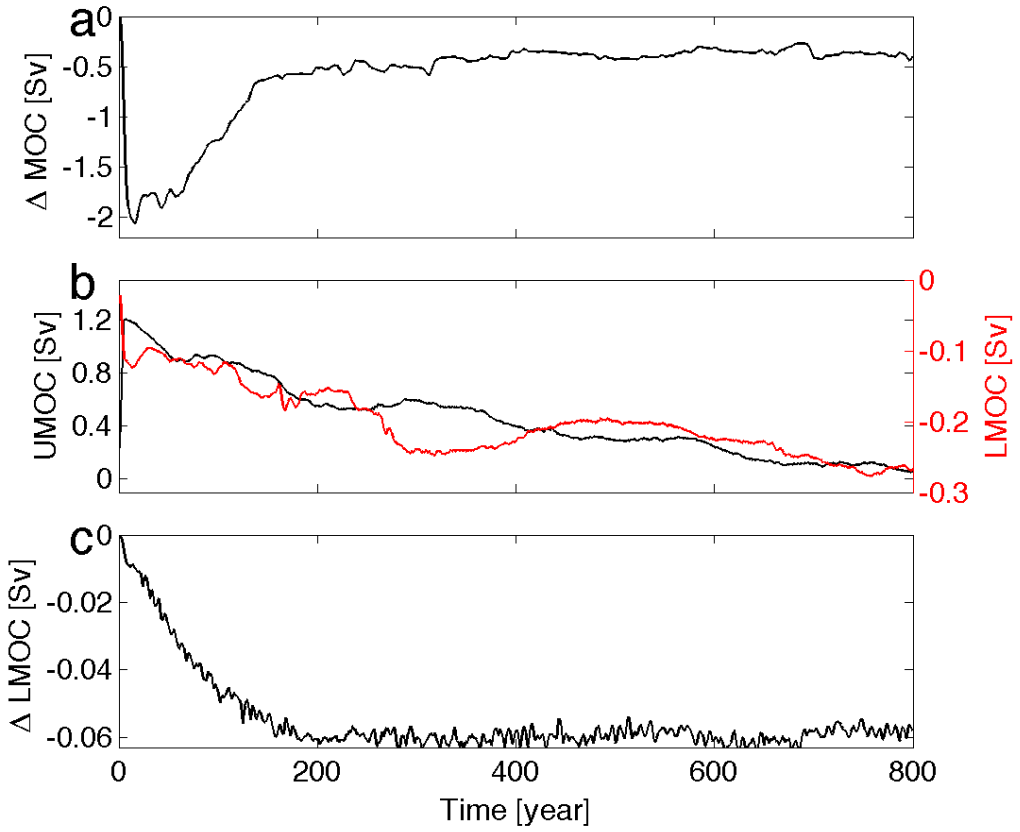

FIG. 7. **(a)** Change of the strength of the upper meridional overturning circulation (ΔUMOC), defined as the maximum meridioal overturning streamfunction in density space, in WN. **(b)** black line: the upper meridional overturning streamfunction (UMOC) averaged within the channel and in the temperature range of 4-5°C in WN; red line: the lower meridional overturning circulation (LMOC) averaged within the channel and below temperature 4°C in WN. Positive value means clockwise circulation, and negative value means counter-clockwise circulation. **(c)** decline of the strength (absolute value) of the lower meridional overturning circulation (ΔLMOC) averaged below temperature 4°C and north of 48°S in WS. This is for the case with $\kappa = 0.5 \times 10^{-5} m^{-2} s^{-1}$ and $\tau_s = 0.2 N m^{-2}$. In WN, the upper MOC cell and the lower MOC cell have continued decline and increase in the channel. In WS, the lower MOC cell is reduced as a consequence of slumping isopycnals. All data are 5-year running average.

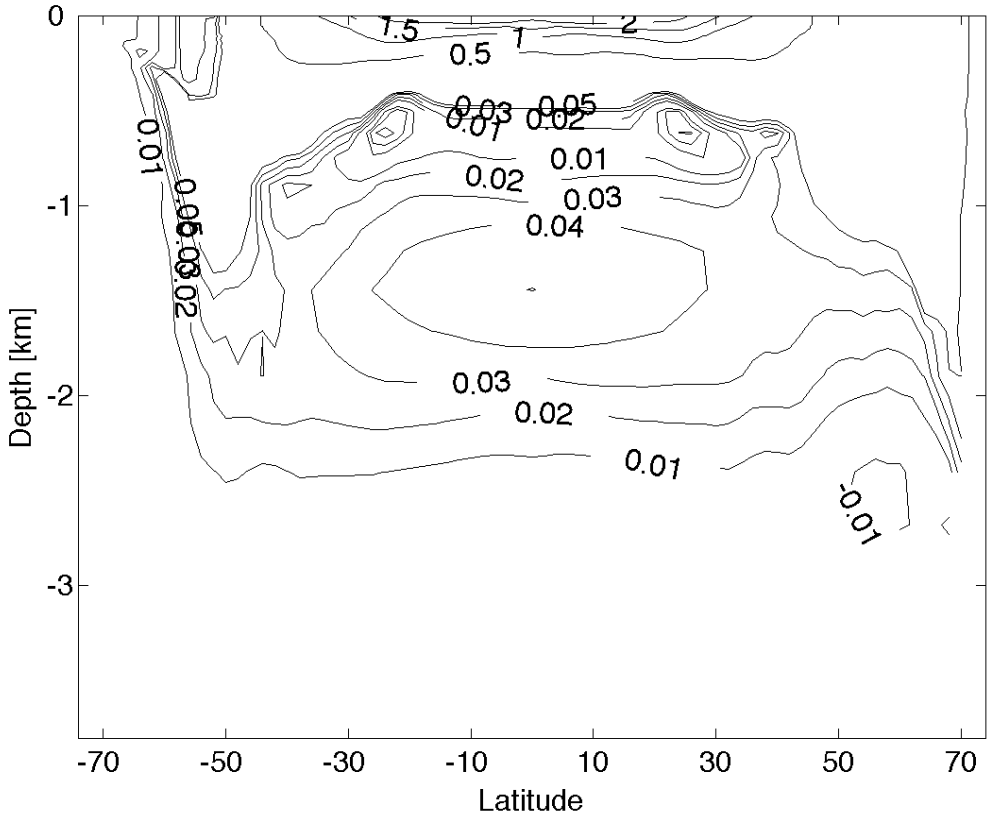

FIG. 8. Contours of temperature change in WM at year 400. Under the warming in low- and mid-latitudes, the mid-depth ocean in conjunction with the upper MOC cell warms up slowly and heat extends southward from northern high latitudes. Contour intervals are 0.5°C above 5 and below -5°C, and 0.01°C in between.

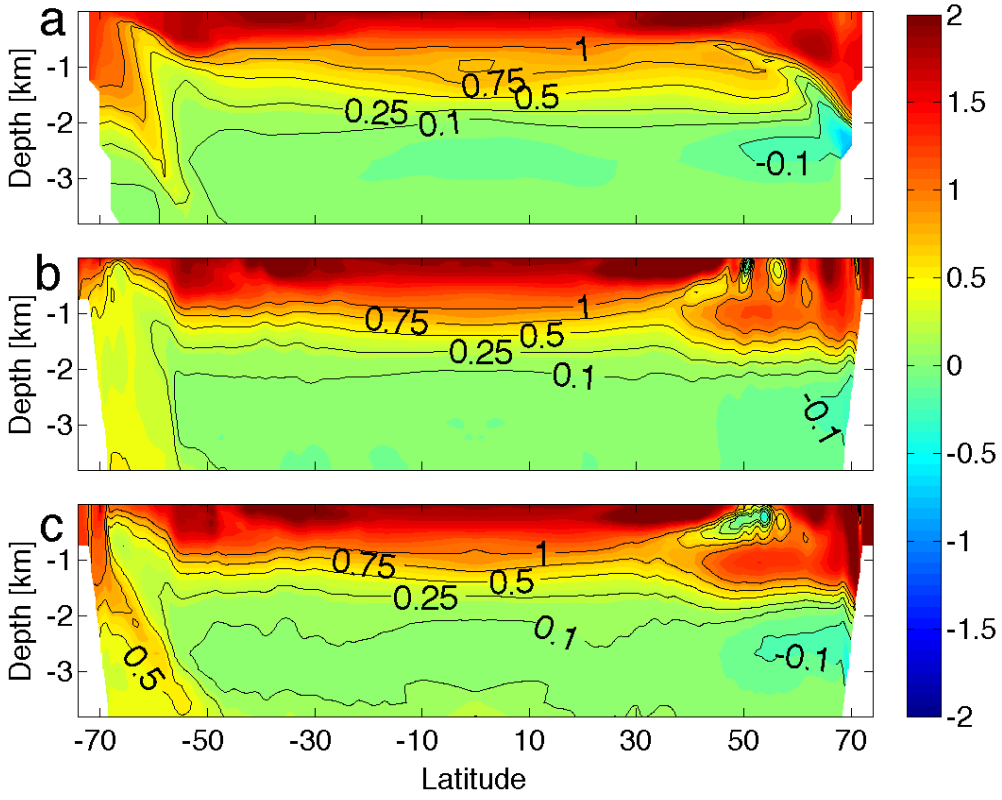

FIG. 9. Change of the zonal mean temperature averaged between year 90-100 in W in the coarse resolution run (**a**), 0.25° run (**b**) and 0.125° run (**c**).

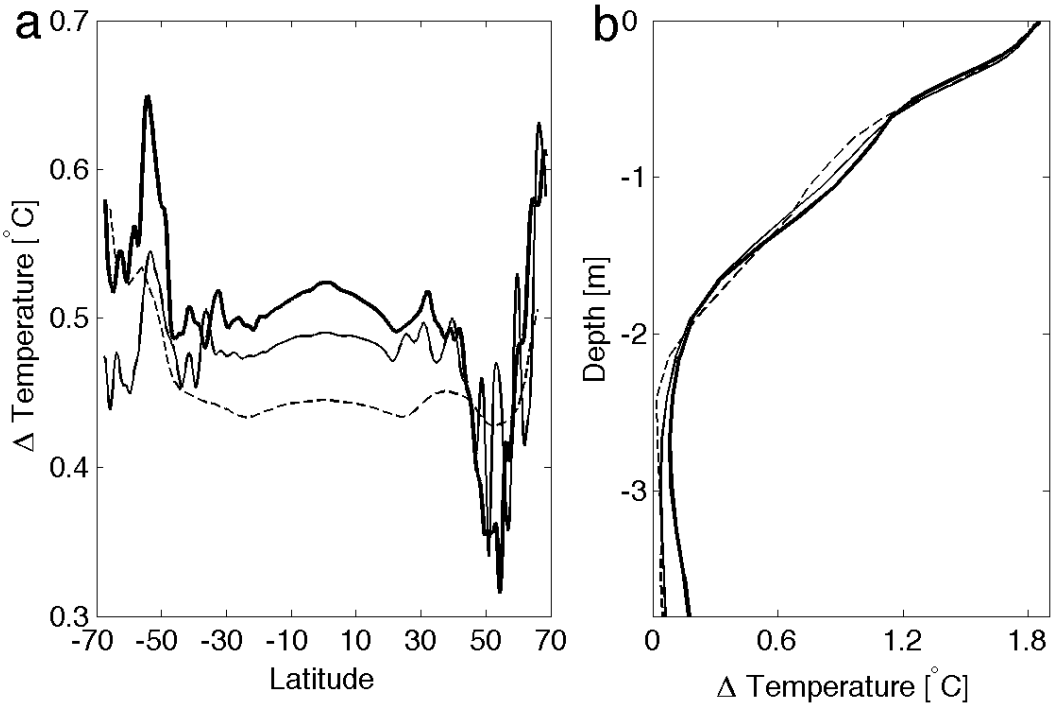

FIG. 10. Latitudinal (**a**) and vertical distribution (**b**) of temperature change averaged between year 90-100 in W in the coarse resolution run (dashed), 0.25° run (solid) and 0.125° run (thick solid). It is noticeable in **a** that the southern high latitude warming is weaker in the eddy-permitting model than in the eddy-resolution model, and the cooling tendency near the polar edge of the subtropical gyre is strongest in the eddy-resolving model. In **b**, the change of heat content is stronger in the abyssal ocean in the eddy-resolving model.

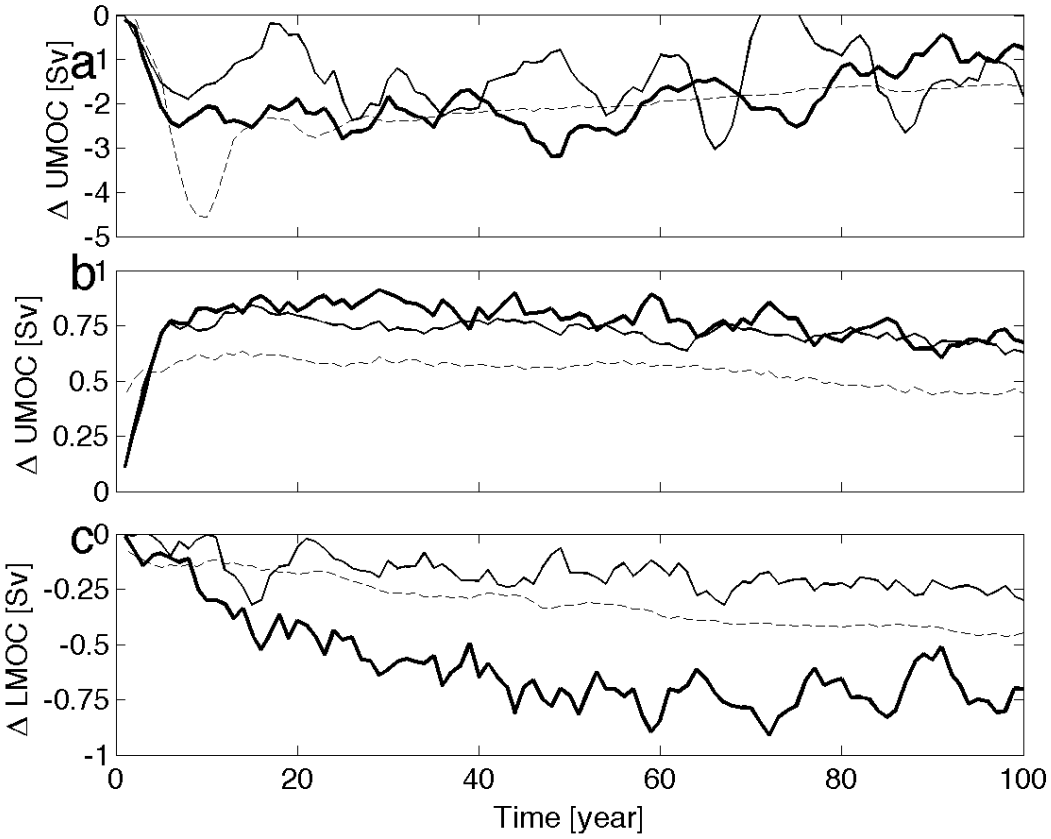

FIG. 11. **(a)** Change of the strength of the upper MOC cell, defined as the maximum strength of the overturning streamfunction in the coarse (dashed), 0.25° (solid) and 0.125° (thick solid) model. **(b)** change of the strength of the upper MOC cell within the channel (65°–55° S), calculated as the average within the range of 5-10°C in the coarse (dashed), 0.25° (solid) and 0.125° (thick solid) model. **(c)** change of the strength of the lower MOC cell (absolute value) within the channel, calculated as the average below 4°C, in the coare (dashed), 0.25° (solid), and 0.125° (thick solid) model. All data are 5-year running average.

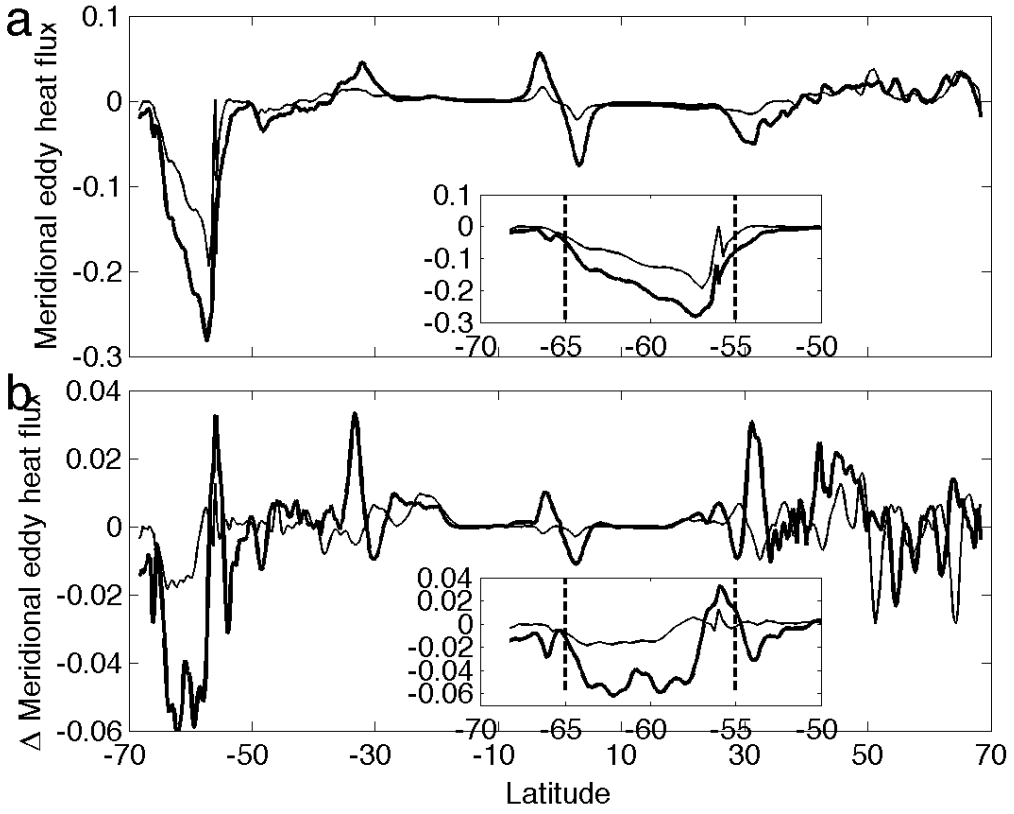

FIG. 12. **(a)** Meridional eddy heat transport normalized by the maximum total meridioal heat transport in CTL in the eddy-permitting (solid) and eddy-resolving model(thick solid). **(b)** change of the meridional eddy heat transport (absolute value) normalized by the maximum total meridional heat transport over all latitudes in W in the eddy-permitting (solid) and eddy-resolving (thick solid) model. All data are averaged between year 90-100. The insets show results between -70°S and -50°S. Thick dashed lines denote the meridional range of the circumpolar channel.

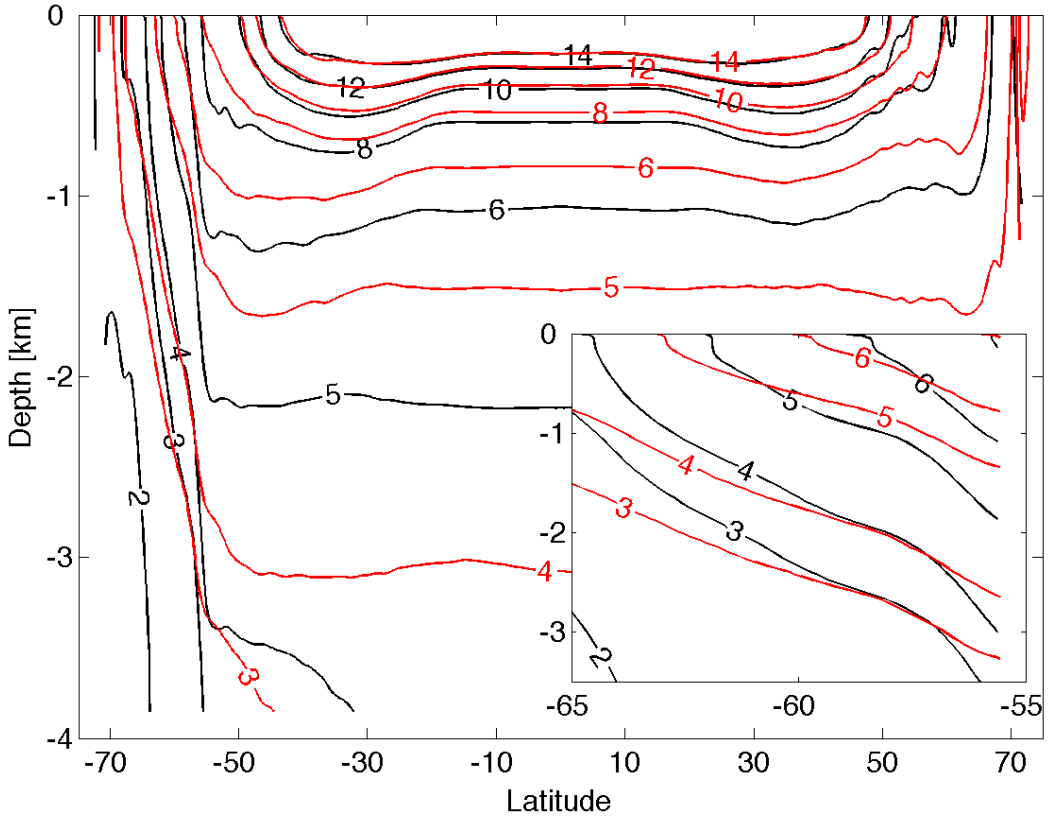

FIG. 13. Time and zonal mean temperature in CTL averaged between year 90-100 in the eddy-permitting (black) and eddy-resolving (red) model. The inset shows the result in the channel.

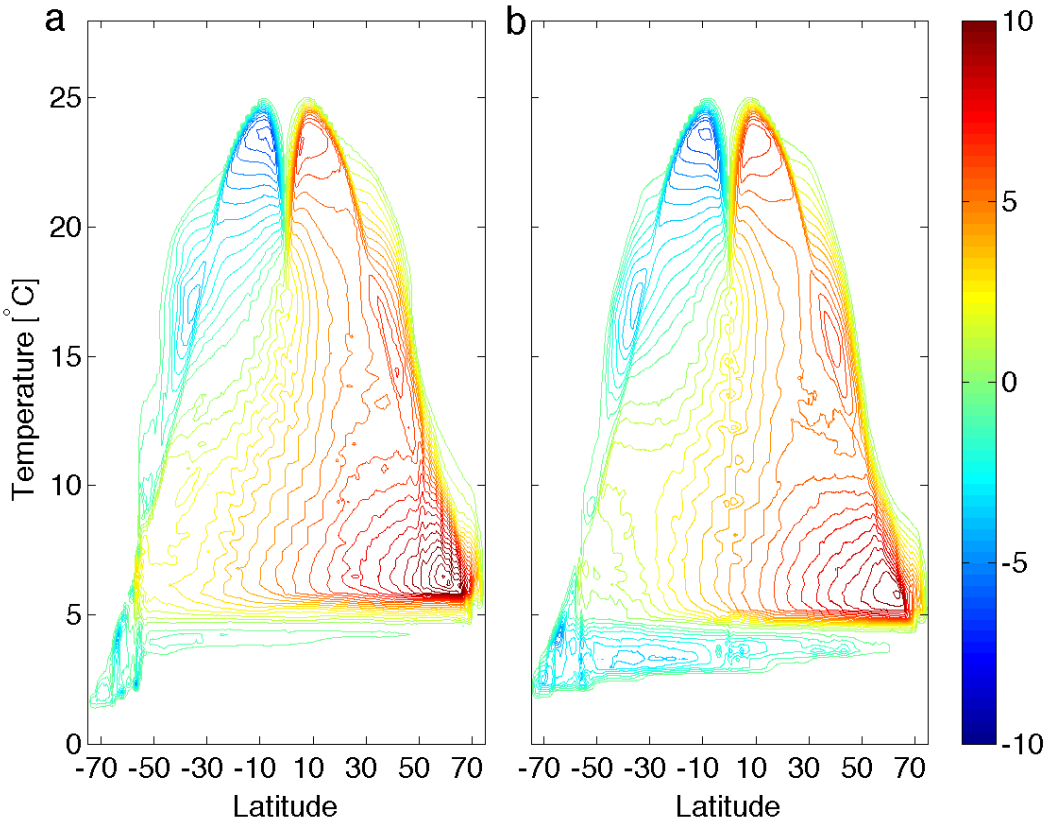

FIG. 14. Meridional overturning streamfunction in density space in CTL averaged between year 90-100 with contour intervals of 0.5 Sv in the eddy-permitting (**a**) and eddy-resolving (**b**) model.

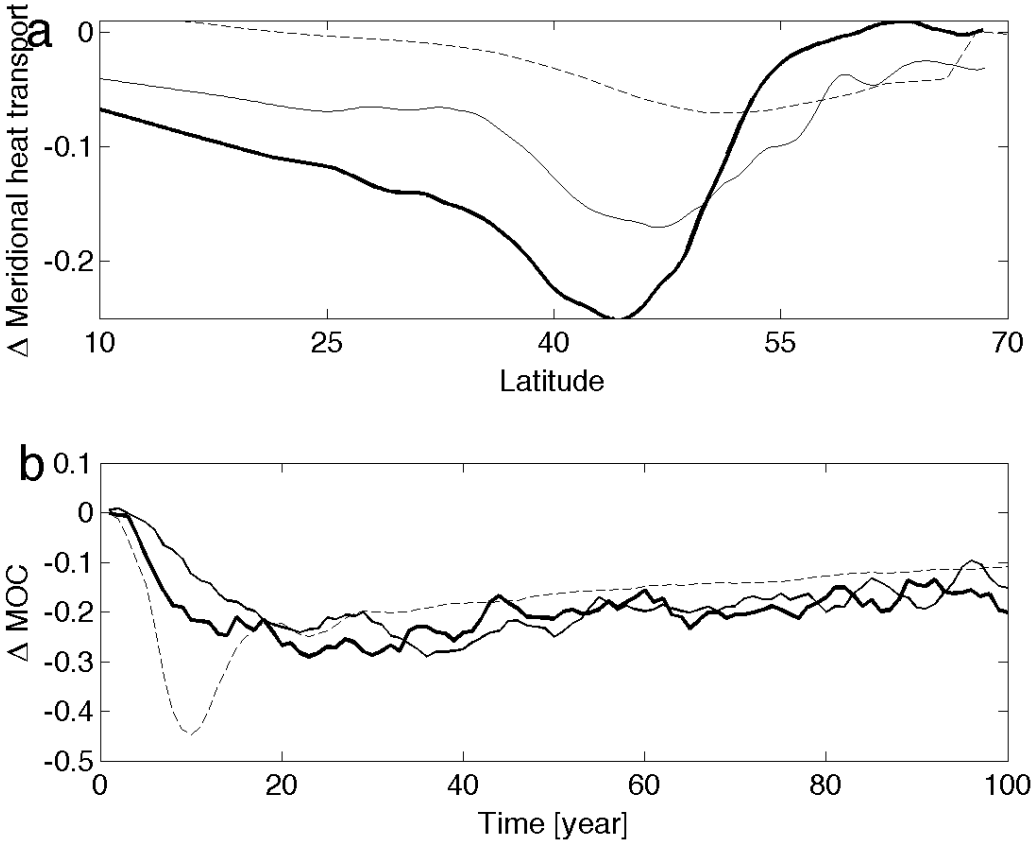

FIG. 15. **a** Change of the total meridional heat transport normalized by its maximum value over all latitudes between year 90-100 in W in the coarse resolution (dashed), eddy-permitting (solid) and eddy-resolving (thick solid) model. **b** Change of the meridional overturning circulation in the coarse resolution (dashed), eddy-permitting (solid) and eddy-resolving (thick solid) model in W. The MOC sterngth is defined as the maximum overturning streamfunction below 10 ° C at each latitude and averaged beween 40°-50° N. The result is then normalized by its time-mean strength in the control climate.

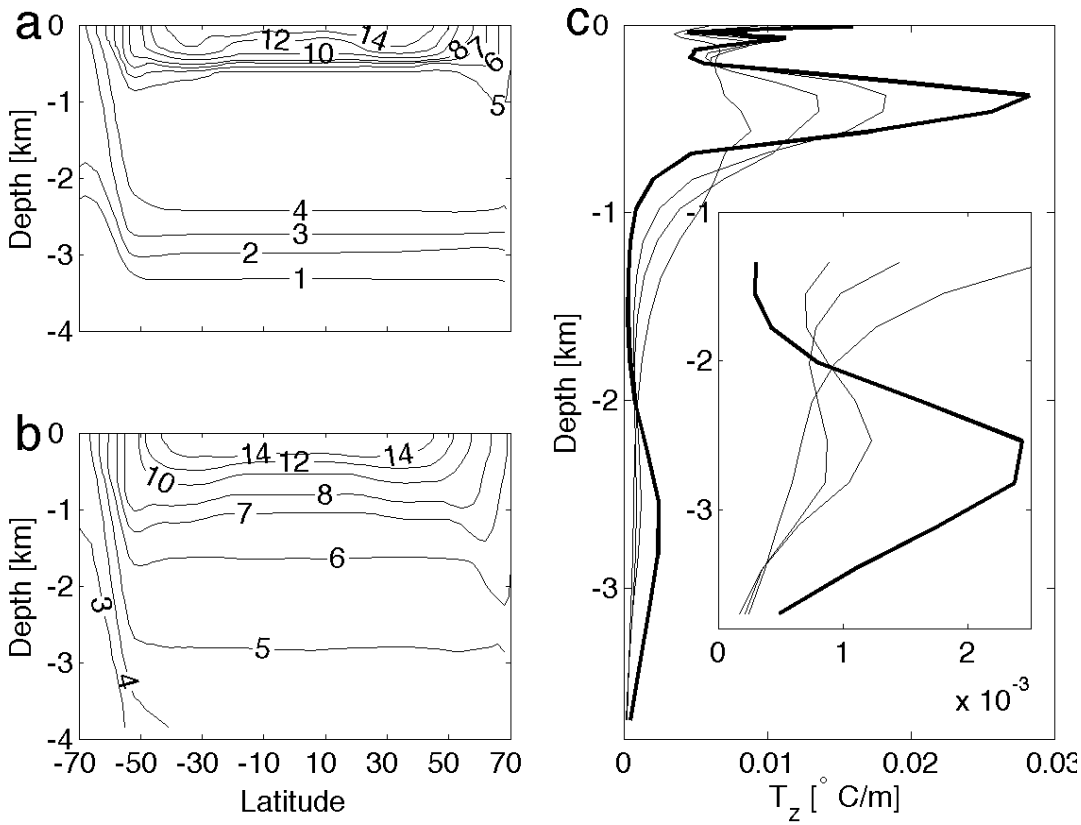

FIG. 16. Zonal and time mean temperature in CTL for $\kappa = 0.1 \times 10^{-5} m^2 s^{-1}$ (**a**) and $6 \times 10^{-5} m^2 s^{-1}$ (**b**). **(c)** vertical gradients of mean temperature for κ =0.5×10^{-5} (thick solid), 2×10^{-5}, 4×10^{-5}, and $10^{-4} m^2 s^{-1}$. The maximum vertical gradient declines with increasing κ.

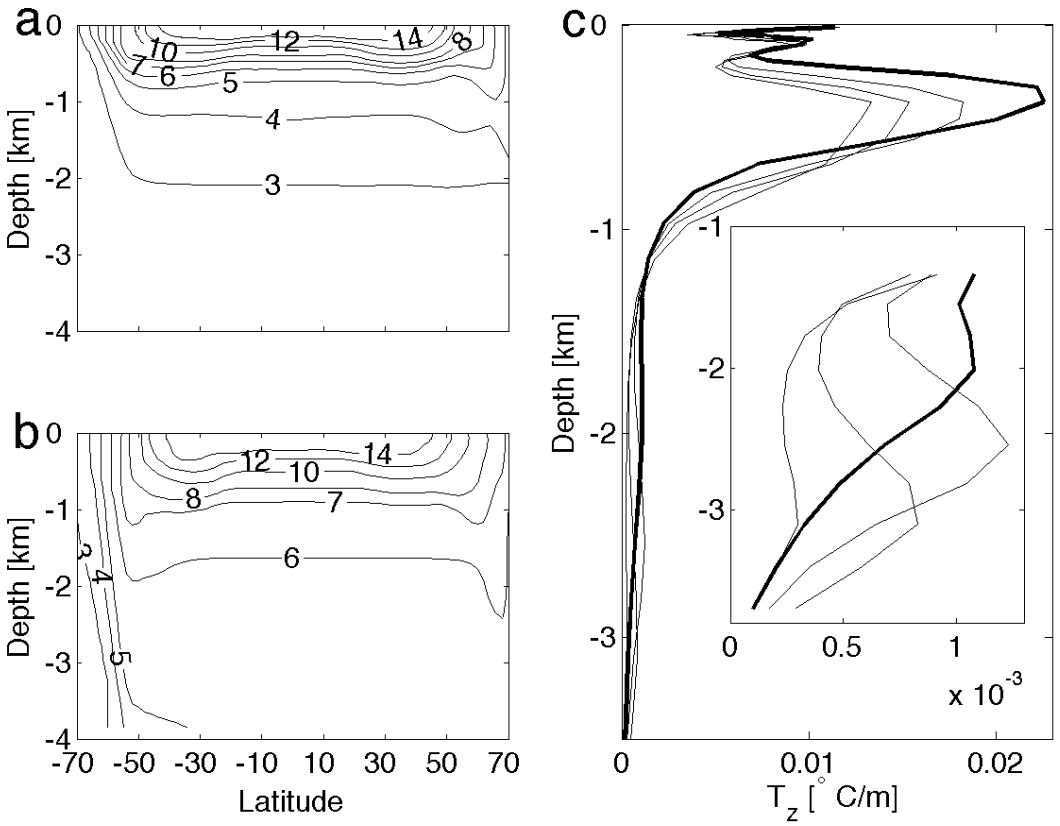

FIG. 17. Zonal and time mean temperature in CTL for $\tau_s = 0.025$ (**a**) and $0.4 Nm^{-2}$ (**b**). **(c)** vertical gradients of mean temperature for τ_s =0.05(thick solid), 0.2, 0.3, and $0.4 Nm^{-2}$. The maximum vertical gradient declines with increasing τ_s.

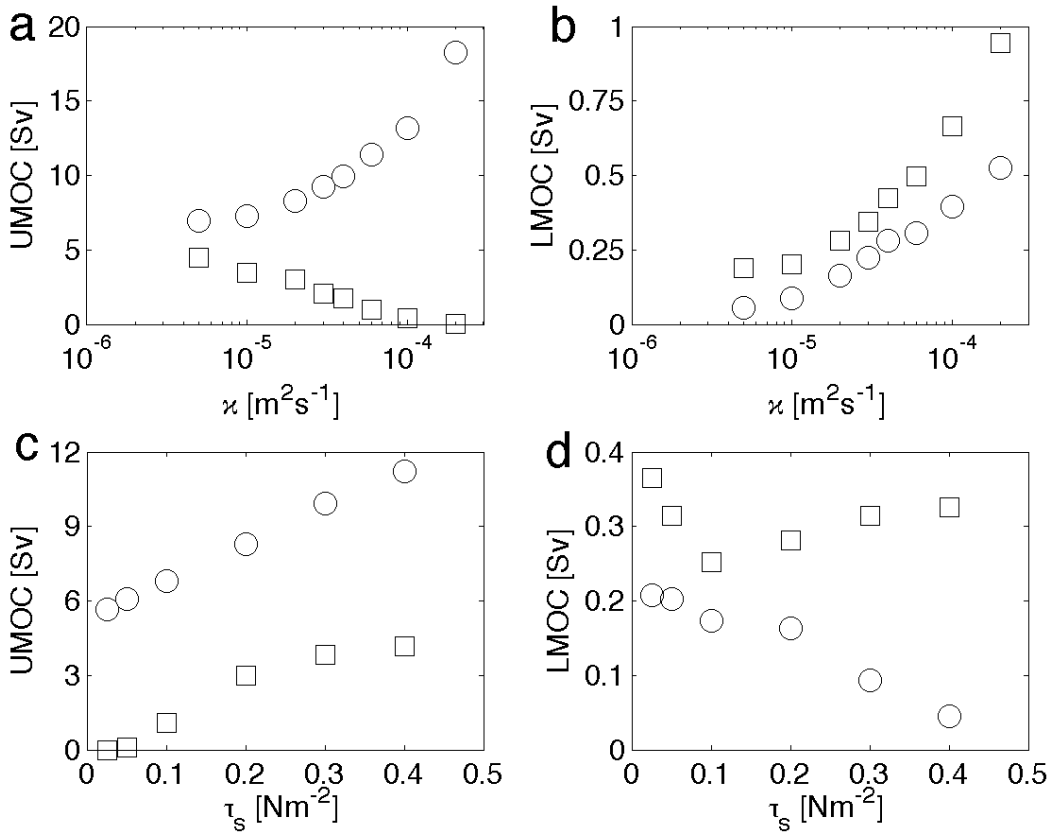

FIG. 18. Meridional overturning circulation in CTL. The rate of the upper meridional overturning circulation in the northern hemisphere (circles) and in the channel (squares) for different κ (**a**) and different τ_s (**c**). The rate of the lower meridional overturning circulation in the northern hemisphere (circles) and in the channel (squares) for different κ (**b**) and different τ_s (**d**).

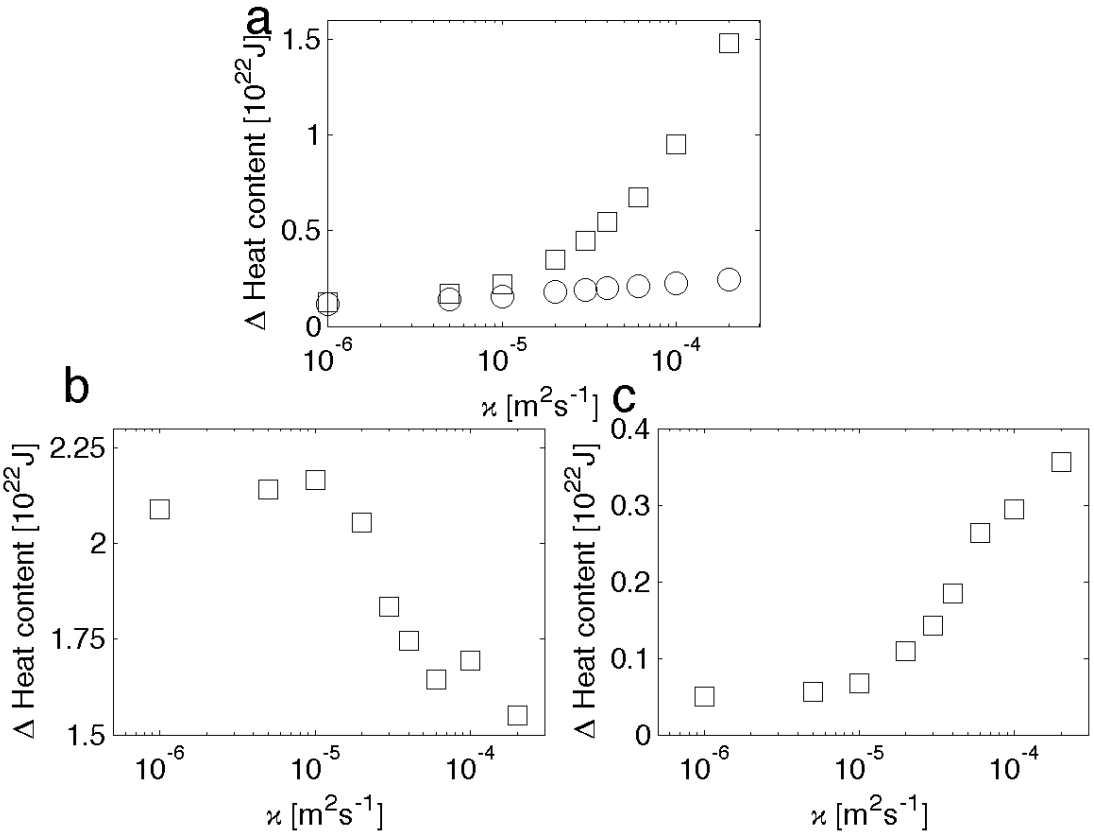

FIG. 19. **(a)** Change of ocean heat content in WM for the entire depth (squares) and above 150 m (circles) at year 800. **(b)** change of ocean heat content in WN at year 800. **(c)** change of ocean heat content in the lower MOC cell in WS and CTL at year 100. Ocean heat uptake at year 100 instead of year 800 is taken for WS in order to have minimum warming within the upper MOC cell.

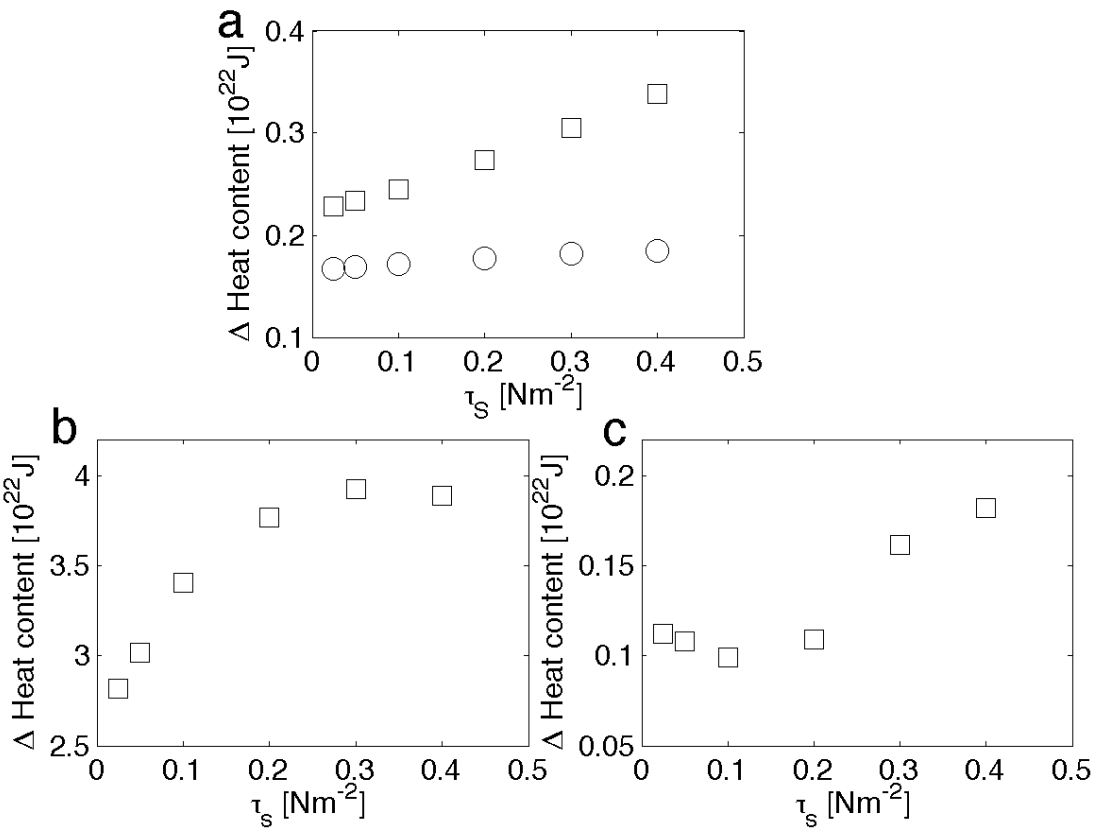

FIG. 20. **(a)** Change of ocean heat content in W for the entire depth (squares) and above 150 m (circles) at year 800. **(b)** change of ocean heat content in WN at year 800. **(c)** change of ocean heat content in the lower MOC cell in WS at year 100. Ocean heat uptake at year 100 instead of year 800 is taken for WS in order to to have minimum warming within the upper MOC cell.

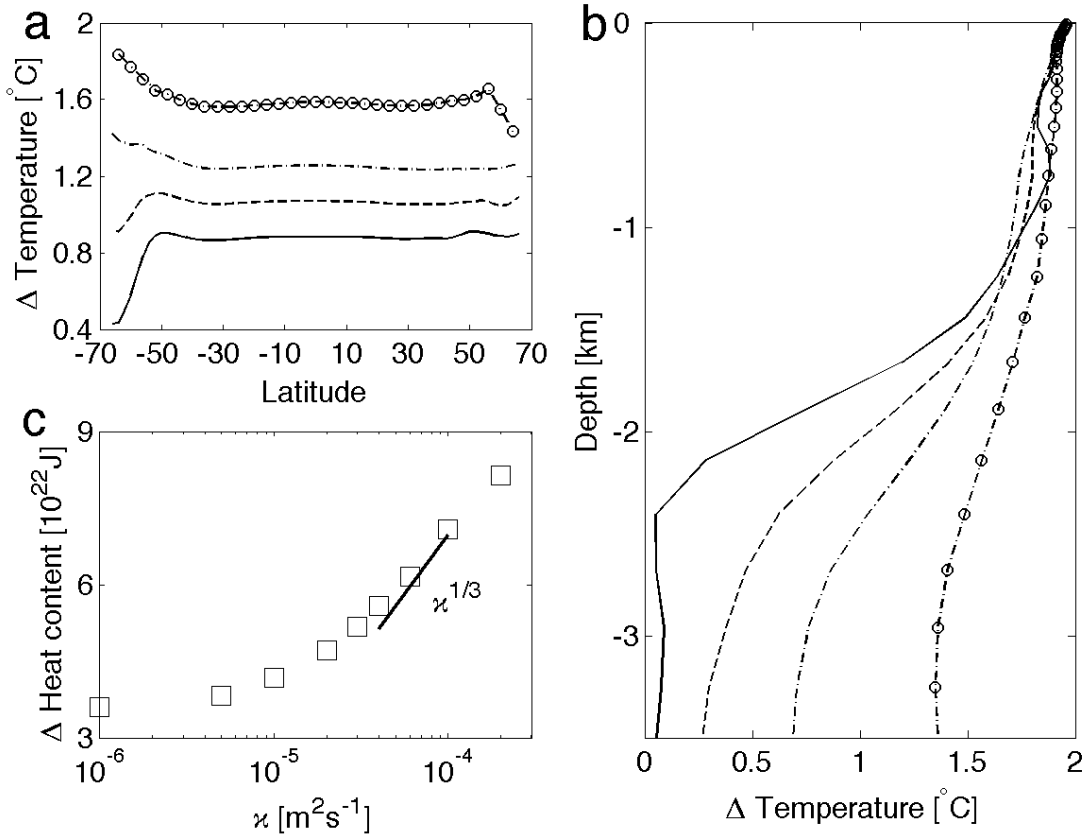

FIG. 21. Meridional (**a**) and vertical (**b**) distribution of change of ocean temperature, and total change of heat content (**c**) at year 800 in W for $\kappa = 0.5\times10^{-5}$(solid), 2×10^{-5}(dashed), 4×10^{-5}(dash-dot), and $10^{-4} m^2 s^{-1}$ (line with circles).

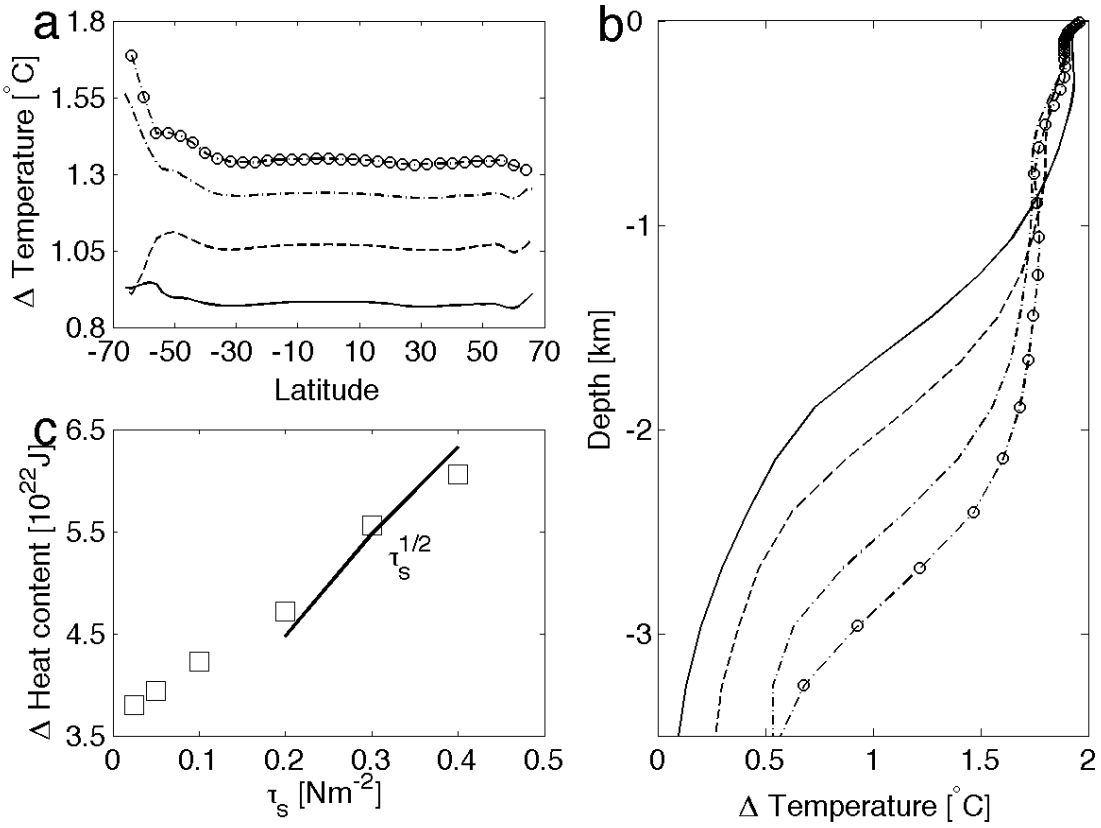

FIG. 22. Meridional (**a**) and vertical (**b**) distribution of change of ocean temperature, and total change of heat content (**c**) at year 800 in W for τ_s =0.05 (solid), 0.2 (dashed), 0.3 (dash-dot), and $0.4 Nm^{-2}$ (line with circles).